



High-Redshift Signatures from the Cosmic Dawn and the Epoch of Reionization

Rennan Barkana¹, Oliver Basquette¹⁷, Ankita Bera², Jennifer Yik Ham Chan^{19,20,21}, Pravabati Chingangbam²⁴, Hector Afonso G. Cruz³, Saswata Dasgupta¹⁷, Kanan K. Datta⁴, Anastasia Fialkov^{17,18}, Sambit K. Giri^{4,5}, Qin Han²², Ilian T. Iliev⁶, Bohua Li⁷, Teppei Minoda⁸, Shikhar Mittal^{9,10}, Julian B. Muñoz¹¹, Suvedha Suresh Naik^{23,24}, Janakee Raste¹⁶, Aurel Schneider¹², Sudipta Sikder¹, Kinwah Wu²², Yidong Xu^{13,14}, Bin Yue^{13,14}, Meng Zhang¹³ and Meng-Lin Zhao¹⁵

¹*School of Physics and Astronomy, Tel Aviv University, Tel Aviv, 69978, Israel*

²*Department of Astronomy, University of Maryland, College Park, MD 20742, USA*

³*Center for Cosmology and Particle Physics, Department of Physics, New York University, New York, NY 10003, USA*

⁴*Department of Physics, Jadavpur University, 188, Raja S.C. Mallick Rd, Kolkata 700032, India*

⁴*Department of Astronomy and Oskar Klein Centre, AlbaNova, Stockholm University, SE-10691 Stockholm, Sweden*

⁵*Van Swinderen Institute for Particle Physics and Gravity, University of Groningen, Nijenborgh 3, 9747 AG Groningen, The Netherlands*

⁶*Astronomy Centre, Department of Physics & Astronomy, Pevensey III Building, University of Sussex, Falmer, Brighton, BN1 9QH, United Kingdom*

⁷*Guangxi Key Laboratory for Relativistic Astrophysics, School of Physical Science and Technology, Guangxi University, Nanning 530004, People's Republic of China*

⁸*Department of Astronomy, Tsinghua University, Beijing 100084, People's Republic of China*

⁹*Battcock Centre for Experimental Astrophysics, Cavendish Laboratory, J. J. Thomson Avenue, Cambridge CB3 0HE, UK*

¹⁰*Kavli Institute for Cosmology, University of Cambridge, Madingley Road, Cambridge CB3 0HA, UK*

¹¹*Department of Astronomy, The University of Texas at Austin, 2515 Speedway, Stop C1400, Austin, Texas 78712, USA*

¹²*Department of Astrophysics, University of Zurich, Winterthurerstrasse 190, 8057 Zurich, Switzerland*

¹³*National Astronomical Observatories, Chinese Academy of Sciences, Beijing 100101, People's Republic of China*

¹⁴*State Key Laboratory of Radio Astronomy and Technology, Beijing 100101, People's Republic of China*

¹⁵*Liaoning Key Laboratory of Cosmology and Astrophysics, College of Sciences, Northeastern University, Shenyang 110819, People's Republic of China*

¹⁶*National Centre for Radio Astrophysics, Tata Institute of Fundamental Research, Pune 411007, India*

¹⁷*Institute of Astronomy, University of Cambridge, Madingley Road, Cambridge, CB3 0HA, UK*

¹⁸*Kavli Institute for Cosmology, Madingley Road, Cambridge, CB3 0HA, UK*

¹⁹*Department of Physics and Astronomy, Oberlin College, Oberlin, OH 44074, USA*

²⁰*Canadian Institute for Theoretical Astrophysics, University of Toronto, 60 St George St, Toronto, ON M5S 3H8, Canada*

²¹*Dunlap Institute for Astronomy and Astrophysics, University of Toronto, 50 St George St, Toronto, ON M5S 3H8, Canada*

²²*Mullard Space Science Laboratory, University College London, Holmbury St Mary, Surrey, RH5 6NT, UK*

²³*Korea Institute for Advanced Study (KIAS), 85 Hoegiro, Dongdaemun-gu, Seoul, Republic of Korea-02455*

²⁴*Indian Institute of Astrophysics, Koramangala II Block, Bangalore 560 034, India*

In this chapter, we provide a comprehensive overview of the astrophysical and cosmological processes that shape the 21-cm signal during Cosmic Dawn and the Epoch of Reionization. We investigate both standard and exotic signatures potentially observable with SKA-Low. Standard signatures are those expected within the Λ CDM framework, including contributions from the first stars, galaxies, and black holes. Exotic signatures are more speculative indicating new physics, such as primordial black holes, modifications to the dark matter sector, non-standard primordial fluctuations, or strongly emitting radio galaxies. The effects of these different sources or scenarios are evaluated in the context of the expected sensitivity of SKA-Low, considering the AA* and AA4 configurations. The chapter aims to provide an overview of the theoretical landscape of 21-cm signatures and to highlight how the forthcoming SKA-Low observations will improve our understanding of astrophysical processes at early times and may open the door towards new physics beyond the Λ CDM framework.

1 Introduction

The redshifted 21-cm signal from neutral hydrogen has emerged as one of the most promising probes of the high-redshift Universe, offering a unique observational window into the epoch of reionization and the preceding cosmic dawn. During this period, the first generations of stars and galaxies emerged, leaving imprints on the intergalactic medium (IGM) that encode both astrophysical processes and potentially new physics.

The evolution of the signal is governed by three main drivers. First, the onset of Lyman- α ($\text{Ly}\alpha$) radiation from the earliest stars couples the hydrogen spin temperature to the gas kinetic temperature via the Wouthuysen-Field effect, making the IGM visible in absorption against the cosmic microwave background (CMB). Second, high-energy X-rays from the first stellar remnants and accreting black holes heat the IGM, transforming the absorption signal into emission as the gas temperature rises above the background. Finally, the growth of ionized regions around galaxies progressively erases the 21-cm signal fluctuations, culminating in the completion of reionization.

Together, these processes produce a rich spectral and spatial signal that not only trace the birth and growth of structure in the Universe, but also provide an indirect laboratory for fundamental physics. It can be used to investigate extensions to the current cosmological model, including the nature of dark matter, exotic energy injection mechanisms, or new interactions beyond the Standard Model. As such, the 21-cm signal is a uniquely powerful probe, bridging astrophysics and fundamental physics at a time when the Universe was less than a billion years old.

The low frequency interferometer of the Square Kilometre Array Observatory (SKA-Low) will provide unprecedented measurements of the frequency range of 50-350 MHz, thereby observing the 21-cm signal at the redshifts $z \sim 6 - 30$. SKA-Low will primarily constrain the signal through power spectrum measurements, allowing the detection of brightness temperature fluctuations at the level of a few milli-Kelvin across a wide range of scales. Forecasts indicate that after a few thousand hours of integration, SKA-Low should be capable of measuring the 21-cm power spectrum with percent-level precision on scales of $0.1-1 h/\text{Mpc}$ during much of the reionization period.

Beyond statistical detections, the high angular resolution and sensitivity of SKA-Low will open the door to tomographic imaging of ionized regions in the mid and late stages of reionization. This would allow direct visualization of the “bubble” morphology driven by early galaxies and quasars, thereby connecting the astrophysical drivers of reionization to the evolving large-scale structure. In combination, these capabilities mean that SKA-Low will transform the study of the high-redshift Universe: delivering not only a detailed astrophysical narrative of cosmic dawn, but also placing tight constraints on exotic physics.

In this chapter we first summarise the physics of the 21-cm signal in the context of SKA-Low (Sec. 2 and 3). We then go on and discuss both signatures from standard, astrophysical (Sec. 4) and from exotic origin (Sec. 5) involving physics beyond the standard model. The standard signatures include early galaxies, Population III stars, X-ray binaries, Cosmic rays, and supermassive black holes. The section furthermore includes a discussion about velocity acoustic oscillations and the polarization of 21-cm radiation. In the exotic signature section we discuss strongly-emitting radio galaxies, primordial magnetic fields, baryon-dark matter interactions, dark matter annihilation and

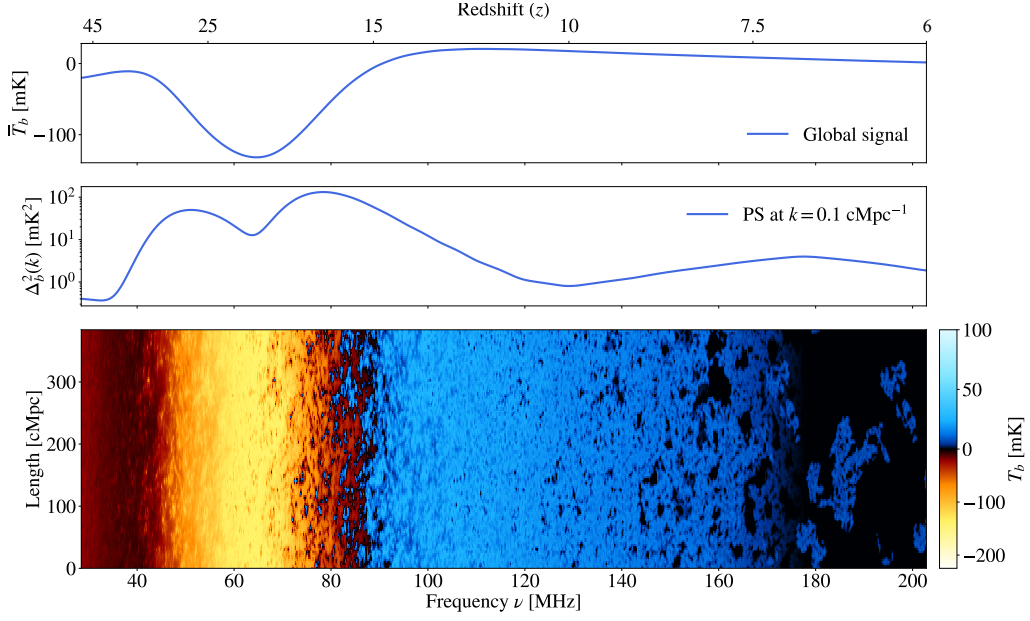


Figure 1: The 21-cm signal across cosmic epochs. The figure illustrates the evolution of the 21-cm signal from the Dark Ages through Cosmic Dawn to the end of the Epoch of Reionization, with reionization completed by $z \sim 6$. **Top:** The sky-averaged (global) 21-cm brightness temperature, \bar{T}_b , as a function of redshift (top x-axis)/frequency (bottom x-axis). The absorption trough at $z \sim 17$ reflects the onset of strong Ly α coupling, followed by X-ray heating and reionization. **Middle:** The 21-cm power spectrum amplitude at $k = 0.1 \text{ cMpc}^{-1}$ showing peaks associated with Ly α coupling, X-ray heating, and ionization fluctuations. **Bottom:** A lightcone map of the differential brightness temperature, T_b , showing the spatial and temporal evolution of the signal. The signal is generated using the code 21cmSPACE (e.g. Gessey-Jones et al., 2025).

decay, non-cold dark matter, and primordial features from inflation. Throughout the whole chapter, we focus on the detectability of all these signatures assuming the AA* and AA4 configurations of the SKA-Low telescope.

2 The physics of the 21-cm signal

We start by providing a summary of the key processes shaping the 21-cm signal and a brief summary of how they are being modelled.

2.1 Lyman- α coupling

During Cosmic Dawn, a strong 21-cm signal is expected in absorption against the CMB as a result of the Wouthuysen-Field (WF) effect (Wouthuysen, 1952; Field, 1958) caused by Ly α photons from the first stars. The WF effect refers to a change in the occupation number of hyperfine states due to resonance scattering of Ly α photons by the hydrogen atom. Stated differently, an electron excited by a Ly α photon may return to a different hyperfine level it originally started from.

Before cosmic dawn, the collisional coupling was the dominant process leading to an absorption signal. As the universe expands, this becomes less efficient and, consequently, there is no contrast with the CMB, which results in a vanishing global signal, as seen at redshift $z \sim 35$ in Fig. 1 (top

panel). Once the first sources turn on, their Ly α radiation once again couples the 21-cm signal to the still-cold gas, resulting in an absorption trough as seen in Fig. 1 at $z \sim 25 - 15$.

The first galaxies are rare and their spatial distribution initially exhibits strong Poisson fluctuations and is later highly clustered, resulting in strong fluctuations in the Ly α background and thus the redshifted 21-cm line (Barkana and Loeb, 2005b). This is evident from the middle panel in Fig. 1 which shows the 21-cm power spectrum (Δ^2) at a representative scale of $k = 0.1 \text{ cMpc}^{-1}$.

The Ly α coupling x_{Ly} depends on the local specific intensity J_α which is expensive to compute. This is due to the large number of scatterings ($\sim 10^6$) occurring in the line core (Loeb and Rybicki, 1999; Baek et al., 2009b) at sub-Mpc scales which must be captured for an accurate model of J_α and hence the Cosmic Dawn signal. Several different approaches have been proposed to deal with this, from analytical ones based on the wing-approximation (Chuzhoy and Shapiro, 2006; Furlanetto and Pritchard, 2006; Mesinger et al., 2011; Mittal and Kulkarni, 2020), semi-numerical ones, where the radial profile ($J = J(\nu, r, z)$) for an idealised source assuming a spherical symmetry is pasted over all the sources in the cosmological box (Reis et al., 2021; Schaeffer et al., 2023), to numerical ones, where a hydrodynamical simulation is post-processed with Monte Carlo radiative transfer simulation (Semelin et al., 2023; Mittal et al., 2024).

It is now well-established that the lack of detailed Ly α radiative transfer can result in modelling biases in the global 21-cm signal and even more so in calculating the 21-cm power spectrum (Reis et al., 2021; Semelin et al., 2023; Mittal et al., 2024). Fluctuations in the Ly α field for a wide range of scales can alter the 21-cm power spectrum by factor of up to a few. For example, consider an idealised Universe with no ionizing or X-ray sources so that the only sources of fluctuations are gas temperature and Ly α coupling. At $k = 0.07 \text{ cMpc}^{-1} h$, we have $\Delta_{21}^2 \approx 217 \text{ mK}^2$ when a rigorous radiative transfer simulation of Ly α is followed and $\Delta_{21}^2 \approx 60 \text{ mK}^2$ at the same wavenumber for no detailed radiative transfer (Mittal et al., 2024). This stronger power spectrum is induced by the additional fluctuation in Ly α coupling. In the middle panel of Fig. 1, the highest redshift peak in the 21-cm power spectrum is caused by fluctuations in J_α . Upcoming experiments such as SKAO are strong candidates for verifying the 21-cm power spectrum for a wide range of scales.

2.2 Heating process

The thermal history of the IGM is a crucial component that drives the behaviour of the 21-cm signal on par with the Ly α coupling (Sec. 2.1) and the process of ionization (discussed in Sec. 2.3). Heating and cooling processes affect the 21-cm signal across the Dark Ages, Cosmic Dawn and the Epoch of Reionization. After recombination, the Universe cools largely adiabatically due to the cosmic expansion. Once it decouples thermally from the CMB at $z \sim 150$ (Seager et al., 1999), the pristine gas, composed primarily of neutral hydrogen and helium, cools more rapidly than the CMB. This results in the IGM being colder than the CMB, which manifests as absorption by hydrogen atoms from the CMB, as shown in the top panel of Fig. 1. The subsequent thermal evolution, however, is shaped by a complex interplay of various other heating and cooling mechanisms that add to this expansion-driven cooling (e.g. Madau et al., 1997; Furlanetto, 2006; Pritchard and Furlanetto, 2007; Baek et al., 2009a; Mesinger et al., 2011; Fialkov et al., 2014; Pacucci et al., 2014; Reis et al., 2021; Gessey-Jones et al., 2023).

Once the first collapsed structures begin to form, several heating mechanisms become important (Kang and Shapiro, 1992; Anninos et al., 1997). Shock heating arises from the gravitational collapse of matter, where supersonic gas flows create shocks that thermalize kinetic energy into heat (Furlanetto and Loeb, 2004). As the first stars form and die, they contribute several additional large-scale heating mechanisms mediated by X-rays (Pritchard and Furlanetto, 2007), cosmic rays (Sazonov and Sunyaev, 2015; Bera et al., 2023; Gessey-Jones et al., 2023), and Ly α photons (Chuzhoy and Shapiro, 2007; Mittal and Kulkarni, 2020; Reis et al., 2021). The Compton heating and cooling from scattering of CMB photons also contributes (Kang and Shapiro, 1992). The first prediction of observable 21-cm fluctuations from inhomogeneous X-ray heating was made by Pritchard and Furlanetto (2007), applying galaxy fluctuations to X-ray emission (instead of Ly α emission which was first discussed by Barkana and Loeb, 2005b).

At cosmic dawn, X-rays are thought to be produced by X-ray binaries (XRBs Power et al., 2013; Fragos et al., 2013b) – binary systems where matter accretes onto a compact object (neutron star or black hole) emitting copious X-rays (see further discussion in section 4.3), and quasars (likely subdominant at the redshifts relevant for the SKAO, Madau et al., 2004). Observations suggest that the bolometric luminosity of X-rays, produced by a population of XRBs, scales linearly with the star formation rate (Grimm et al., 2003; Mineo et al., 2012, 2014) – the dependence adopted in numerical simulations and semi-analytical modelling (Pritchard and Furlanetto, 2007; Santos et al., 2008; Mesinger et al., 2011; Fialkov et al., 2014; Ross et al., 2017; Eide et al., 2018). In addition to the total intensity, the shape of the X-ray spectral energy distribution (SED) is an important property (e.g. Fialkov et al., 2014; Ross et al., 2017), as the mean free paths of X-rays in neutral IGM depend on their energy. X-rays with energies between $\sim 0.5 - 2$ keV travel great distances, contributing to the large-scale heating of the IGM (e.g. the mean free path of 1 keV photons in the neutral IGM at $z = 14$ is ≈ 180 comoving Mpc). These X-rays also contribute to large-scale patterns of partial ionization in the IGM (up to 10%, Baek et al., 2010; Pacucci et al., 2014; Fialkov et al., 2017). Lower-energy photons ($\lesssim 0.5$ keV) are absorbed locally at the source, while the more energetic X-rays are not absorbed at all, thus contributing to the cosmic X-ray background (e.g. Fragos et al., 2013b; Fialkov et al., 2017; Ma et al., 2018).

Another proposed heating source, which competes with X-rays, is heating by cosmic rays, primarily produced by supernovae within the first galaxies (Sazonov and Sunyaev, 2015; Bera et al., 2023; Gessey-Jones et al., 2023). While cosmic rays have shorter mean free paths compared to X-rays and deposit their energy very close to the sources, cosmic rays can still contribute significantly to local heating, particularly in the vicinity of star-forming regions. For the further discussion of cosmic ray heating see section 4.4.

One more heating mechanism that is crucial at cosmic dawn is the Ly α heating. Along with mediating the coupling of spin temperature T_S to the kinetic temperature T_K , the Ly α photons also exchange energy with the hydrogen atoms through repeated scattering (Chen and Miralda-Escudé, 2004; Chuzhoy and Shapiro, 2007; Ciardi et al., 2010; Mittal and Kulkarni, 2020; Reis et al., 2021; Raste et al., 2024). Ly α heating is a critical and non-negligible component in shaping the thermal history of IGM, which might compete with X-ray heating (Reis et al., 2021; Mittal et al., 2026). Despite its importance, this heating term is often overlooked.

These competing heating and cooling processes profoundly shape the observable redshifted 21-cm signal. The 21-cm signal (Fig. 1) traces the contrast between the IGM temperature and that of the radio background radiation (often assumed to be the CMB). As soon as the considerable population of first heating sources is formed, it acts to reduce the contrast between the IGM and the CMB temperatures, eventually heating the IGM above the temperature of the CMB. This action is directly visible in the global 21-cm signal (top panel, Fig. 1), which transitions from a deep absorption trough into an emission bump (although if heating is inefficient, the signal remains in absorption [Fialkov et al., 2014](#)).

The spatial fluctuations in the IGM temperature and ionization state, driven by these heating mechanisms, are imprinted on the 21-cm signal (bottom panel, Fig. 1). For instance, inhomogeneous X-ray heating creates large-scale temperature fluctuations that can dominate the 21-cm power spectrum at intermediate redshifts $z \sim 10 - 20$ (middle panel, Fig. 1), offering a unique probe of the sources and efficiency of early universe heating ([Pritchard and Furlanetto, 2007](#)). Understanding and modelling these heating processes is thus paramount for interpreting the 21-cm observations with the SKA.

2.3 Ionization process

The reionization process is complex, driven by a variety of ionizing sources. The photon production was likely dominated by softer-spectrum stellar sources, likely with some contribution from harder ones like QSOs and X-ray binaries. It has now been established that the process is inside-out, i.e. denser regions are reionized on average earlier, with reionization starting from the high-density peaks, where the early galaxies form, and gradually expanding outwards, with the largest, deepest, emptiest voids reionizing last ([Barkana and Loeb, 2004](#); [Furlanetto et al., 2004](#); [Iliev et al., 2006](#); [Giri et al., 2024](#); [Choustikov et al., 2025](#)). Furthermore, according to the statistics of the peaks of a Gaussian field, early, rare sources tend to cluster together. Low-mass sources could be suppressed by radiative feedback, thereby boosting the importance of the larger, more clustered sources. Finally, the effect of absorbers, specifically Lyman-limit systems ([Shukla et al., 2016](#)) and unresolved gas density fluctuations that increase the recombination rate, is to slow and extend reionization, while also breaking up the ionized patches into smaller ones ([Bianco et al., 2021](#); [Choudhury and Chakraborty, 2025](#)). Therefore, the reionization patchiness encodes a wealth of information about the nature, abundance and clustering of the early galaxies and the properties of the IGM.

The ionizing sources and sinks, and the resulting reionization history and morphology are reflected in the redshifted 21-cm signal and can thus be constrained by it. The detailed dependencies are complex, and subject of ongoing studies, but certain general trends have become clearer. More efficient feedback and suppression of the lower-mass sources increase the relative contribution of the massive sources. The latter are rarer and more clustered, yielding larger, smoother ionized patches. This boosts the large-scale 21-cm power and moves the peak of the 21-cm rms fluctuations to larger scales and lower redshifts, making the detection of these signals easier since SKA is more sensitive there, while foregrounds are weaker at late times. In contrast, a less efficient feedback would increase the contribution of the much more numerous low-mass sources, thereby extending the reionization process and producing larger number of smaller ionized patches, making detection more difficult ([Iliev et al., 2012](#)). The same is true also for the tracking of the mean reionization

history (see Fig. 1 for an example), where a shorter and sharper ‘step’ would significantly facilitate detection. Other effects like the spectra of the dominant source population (e.g. Gessey-Jones et al., 2023; Ma et al., 2023), metal enrichment and the transition from metal-free to later generations of stars, and even source radiation anisotropy (Schwandt et al., 2025) have also been considered.

Many redshifted 21-cm line signatures have been investigated over the last 30 years, from the global mean reionization history (e.g. Mondal et al., 2019), through statistical measures like the power spectra, 1-point (PDFs, rms, skewness) and 2-point (bispectra) statistics (Iliev et al., 2006; Giri et al., 2019a; Shaw et al., 2019; Noble et al., 2024; Muñoz and Cyr-Racine, 2021), line-of sight effects (e.g. Jensen et al., 2013; Mondal et al., 2020; Ross et al., 2021; Th  lie et al., 2025), to direct imaging (e.g. Giri et al., 2018, 2019b; Zackrisson et al., 2020). The ionizing photon sinks can also have considerable effect on the 21-cm signatures. During EoR the ionizing photons typically do not travel very far from their emitting galaxy and are absorbed by the nearest neutral patch. However, towards and after overlap, such patches become rare and the mean free path of the ionizing photons rises dramatically (Lewis et al., 2022; Satyavolu et al., 2024), set by the abundance and nature of the remaining absorbers, Lyman-limit and Damped Ly α systems. Furthermore, most of the neutral hydrogen at that epoch is found in the same absorber systems. Consequently, they directly influence the 21-cm power spectra and other related observables and should be included in any realistic modelling, particularly of the tail-end of reionization and post-reionization IGM (Shukla et al., 2016; Bianco et al., 2021; Giri et al., 2024; Fan et al., 2025; Georgiev et al., 2025).

The links between the early galaxies and the 21-cm signal are complex, and thus linking them reliably requires realistic modeling. Models range from the cheaper and faster, but inevitably more approximate semi-numerical approaches (e.g. Fialkov et al., 2014), through simplified simulations (Ghara et al., 2018), to full and thus more expensive radiative transfer (Mellema et al., 2006; Hirling et al., 2024) and fully coupled radiative hydrodynamics numerical simulations (Ocvirk et al., 2020). Machine learning methods are used to construct fast emulators and thus to further accelerate parameter searches and fitting (e.g. Ghara et al., 2020). Currently the parameter space searches and fitting is largely limited to the fast, semi-numerical approaches and simplified simulations, and emulators based on such modelling, but with the advent of GPUs and improved numerical methods even full radiative transfer methods are becoming viable for this (Hirling et al., 2024).

2.4 Accurate 21-cm line transfer for SKA-Low tomographic studies

SKA-Low’s 21-cm tomographic data are light-cone measurements. An observed frequency picks up photons that redshifted into that band after being emitted at specific cosmic time. Each channel is therefore a path-integrated record of the cosmological medium they traversed. As radiation travels through the expanding, inhomogeneous Universe, it undergoes emission and absorption, and interacts with ambient radiation fields, such as the CMB radiation and any background and ambient radiation in the bands. The CMB is not merely a continuum that the 21-cm signal is observed against. It contributes to setting the radiation temperature, T_r , and it regulates absorption and emission through radiative (stimulated) transitions. Additional radio background would alter this balance. The cosmological 21-cm line radiative-transfer is not simply a convolution. The measured signal encodes the cumulative, frequency-dependent imprints of hydrogen density, gas velocities, and radiation fields along its path. As such, the radio transfer of the 21-cm line is required to be

self-consistent in the joint (z, ν) domain. A resolution is to adopt the cosmological 21-cm line radiative transfer (C21LRT) formulation. The corresponding C21LRT equation for the intensity of the 21-cm line, $I_{L,\nu}$, along the photon path s would take the form:

$$\frac{d}{dz} \left(\frac{I_{L,\nu}}{\nu^3} \right) = (1+z) \left[-(\kappa_{C,\nu} + \kappa_{L,\nu} \phi_\nu [1 - \Xi]) \left(\frac{I_{L,\nu}}{\nu^3} \right) + \frac{(\epsilon_{C,\nu} + \epsilon_{L,\nu} \phi_\nu)}{\nu^3} \right] \frac{ds}{dz}, \quad (1)$$

(Chan et al., 2024; Wu et al., 2024), with the subscript ‘‘L’’ denoting the line centre and ‘‘C’’ the continuum underneath and neighbouring to the line. The factor $[1 - \Xi]$ accounts for stimulated emission. The increment of path length with respect to the change in redshift, ds/dz , is set by the assumed cosmological model. The line absorption and emission coefficients ($\kappa_{L,\nu}$ and $\epsilon_{L,\nu}$) are determined by the Einstein coefficients, and the number densities of HI in the two hyperfine states.

The observed 21-cm spectral signal can be expressed either as the specific intensity contrast, $(I_{L,\nu} - I_{C,\nu})$, or as the differential brightness temperature, $\delta T_b = (I_{L,\nu} - I_{C,\nu})(c/\nu)^2/(2k_B)$. This general expression makes no assumptions regarding the optical depth, spatial uniformity of the neutral hydrogen gas, nor linearity in the velocity field.

The accurate modeling of 21-cm tomographic signals that interface simulated fields like ionized fraction, gas density, velocity and temperature with C21LRT to produce light-cone spectral cubes. These are then propagated through the SKA measurement equations to generate 21-cm model templates. This modeling approach will enable more proper and accurate comparisons to observational data. It will also provide data test-beds to deliver better and more reliable inference of reionization history, bubble size distributions, and the thermal evolution of the gas.

3 SKA observational setup

We assess the capability of SKA-Low to measure key cosmological and astrophysical signatures by evaluating and comparing its proposed AA* and AA4 antenna layouts. Our analysis considers three primary sources of contamination:

- **Cosmic variance:** This statistical uncertainty is dictated by the finite volume of the observable universe, which is limited by the size of the primary beam. The beam size can be approximated as $21\text{cm}(1+z)/D$, where D represents the diameter of an individual antenna station. For this study, we adopt a station diameter of 38 m.
- **Instrumental noise:** This source of error is influenced by the telescope’s design, including antenna sensitivity and array layout, as well as specific observational parameters. See, e.g., Mellema et al. (2013) and Giri et al. (2018) for a more detailed discussion on these parameters. We evaluate the AA* configuration (307 stations) and the AA4 configuration (512 stations). For both layouts, we adopt a fiducial setup with a total integration time of 1080 hours, a bandwidth of 10 MHz, and a power spectrum binning of $\Delta \ln k = 0.5$.
- **Foreground Contamination:** Bright astrophysical foregrounds represent the most significant challenge. A common strategy to mitigate their impact on the 21-cm power spectrum is to apply a scale cut, removing the Fourier modes most affected by foreground leakage. We

adopt a conservative cut at $k \lesssim 0.15 \text{ Mpc}^{-1}$ (Poher et al., 2014). We should note that some signatures, such as the velocity acoustic oscillations (Sec. 4.6), are found at larger scale and would require sophisticated foreground mitigation. For a more comprehensive discussion on foregrounds, we refer the interested reader to the [SKA foregrounds chapter \(2025\)](#).

These mock observations can be generated using publicly available software packages that incorporate the latest SKA layouts, such as 21CMSENSE¹ (Murray et al., 2024), TOOLS21CM² (Giri et al., 2020), and KARABO³ (Sharma et al., 2025).

4 Standard Signatures

Here we summarize the main redshifted 21-cm signatures expected within the Λ CDM framework.

4.1 Early galaxies and their properties

Early galaxies, formed within the first billion years of cosmic history, critically influenced the thermal and ionization states of the IGM during the Cosmic Dawn and the EoR (e.g. Bouwens et al. 2015; Muñoz et al. 2022). Characterized predominantly by low metallicities ($Z \ll Z_\odot$) and high specific star formation rates (sSFR) (Ceverino et al., 2018), these galaxies hosted massive, short-lived stellar populations emitting copious amounts of X-ray, Ly α and UV ionizing photons. The interaction of these photons with neutral hydrogen in their surroundings left distinctive imprints observable as redshifted 21-cm emission and absorption signals, providing unique probes into the astrophysical processes operating during these epochs.

Establishing robust links between detailed properties of primordial galaxies and observable 21-cm signatures remains an essential objective in contemporary cosmological research. In this regard, the SKA aims to achieve unprecedented sensitivity and spatial resolution to measure the 21-cm fluctuations across a wide range of redshifts. This observational capability will enable stringent tests of galaxy formation and evolution models, and deeper insights into the feedback processes operating between early galaxies and the IGM. Particularly, in regular EoR galaxy surveys, only the “tip of the iceberg” (the few brightest ones among all the population) has been observed. The majority of the EoR galaxy population is below the detection limit and their properties are largely unknown (Yue et al., 2016, 2018). In contrast, the SKA observations will allow us to reveal the properties of these faint galaxies, as they dominate the ionizing photons budget (Santos et al., 2011; Qin et al., 2021).

The observable features of the 21-cm signal are intricately tied to galaxy-specific parameters (Greig and Mesinger, 2015). The primary ones are star formation efficiency f_\star and escape fraction of ionizing radiation f_{esc} . Motivated by matching the observed high- z UV LFs by HST and JWST, the star formation efficiency f_\star can be parameterized as (Yang et al., 2003)

$$f_\star(M_h) = \frac{2\epsilon_0}{(M_h/M_p)^{-\gamma_{\text{lo}}} + (M_h/M_p)^{\gamma_{\text{hi}}}}. \quad (2)$$

¹<https://github.com/rasg-affiliates/21cmSense>

²<https://github.com/sambit-giri/tools21cm>

³<https://github.com/i4Ds/Karabo-Pipeline>

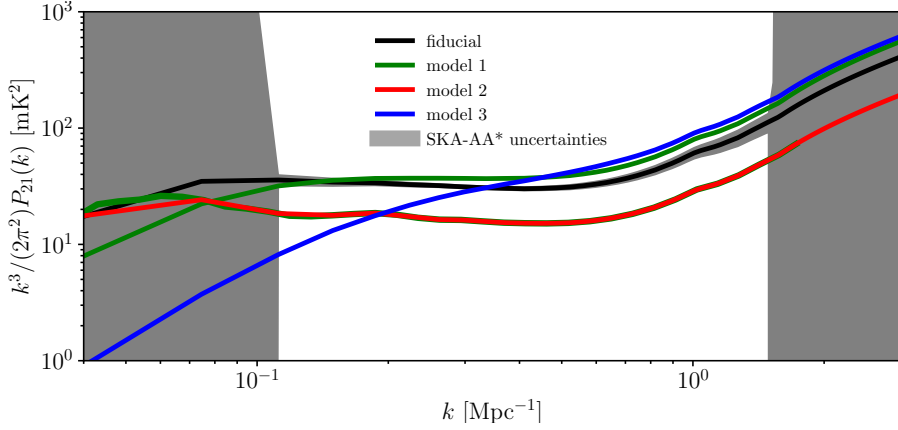


Figure 2: The 21-cm power spectrum at $z \sim 8$ for different parameters in $f_{\star} - M_h$, $f_{\text{duty}} - M_h$ and $f_{\text{esc}} - M_h$ relations. Fiducial model: $\epsilon_0 = 0.13$, $\gamma_{\text{lo}} = 0.46$, $\gamma_{\text{hi}} = 0.82$, $M_p = 2 \times 10^{12} M_{\odot}$, $M_{\text{turn}} = 5 \times 10^8 M_{\odot}$, $M_{\text{esc},0} = 10^{10} M_{\odot}$, $f_{\text{esc},0} = 0.1$ and $\alpha_{\text{esc}} = 0.5$. Model 1: $M_{\text{turn}} = 2 \times 10^8 M_{\odot}$ and $M_{\text{esc},0} = 3.2 \times 10^9 M_{\odot}$, others same to fiducial model. Model 2: $\epsilon_0 = 0.02$ and $\gamma_{\text{lo}} = 0.17$, others same to fiducial model. Model 3: $\epsilon_0 = 0.25$, $\gamma_{\text{lo}} = 0.70$ and $M_{\text{turn}} = 2 \times 10^8 M_{\odot}$, others same to fiducial model. The filled region is the SKA-AA* uncertainties with $t_{\text{obs}} = 1080$ hr and a bandwidth of 10 MHz, calculated by using 21cmSense, assuming moderate foreground removal model.

This formalism, though very simple, reveals an essential fact that star formation is sensitive to feedback: for halos with $M_h \ll M_p$ the supernova feedback dominates, while for halos with $M_h \gg M_p$ the AGN feedback dominates. Moreover, star formation mode in halos close to $T_{\text{vir}} \sim 10^4$ K is bursty, at a given redshift snapshot, only a fraction of halos host active star formation. This is modelled as a duty cycle (Park et al., 2019)

$$f_{\text{duty}}(M_h) = \exp(-M_{\text{turn}}/M_h). \quad (3)$$

When M_h increases to $\sim 10^8 - 10^9 M_{\odot}$, f_{duty} approaches to unity (e.g. Jaacks et al. 2012; O’Shea et al. 2015). The escape fraction of ionizing photons, by contrast, is higher for smaller halos, also partially due to supernova feedback. A parameterization is (Park et al., 2019)

$$f_{\text{esc}} = f_{\text{esc},0} (M_h/M_{\text{esc},0})^{-\alpha_{\text{esc}}}, \quad f_{\text{esc}} \leq 1. \quad (4)$$

The variations of above parameters affect the spatial characteristics of the 21-cm brightness temperature fluctuations, e.g. the power spectrum. Fig. 2 shows the 21-cm power spectra for various parameters in the relations, compared with the SKA-AA* observational uncertainties. Inference of parameters from SKA observed 21-cm power spectrum will build the $f_{\star} - M_h$, $f_{\text{duty}} - M_h$ and $f_{\text{esc}} - M_h$ relations, and further derive the information of metallicity and initial mass function of stellar populations in early galaxies.

Deeper interpretation of the SKA observations will require to develop semi-analytical models (SAMs) that are more sophisticated than above phenomenological model (e.g. Ma et al. 2023). Since the relations between feedback mechanisms in SAMs and the 21-cm signal are rather complicated, machine learning would be helpful for bridging them and extract advanced information from SKA observed 21-cm power spectrum.

4.2 Pop III stars in minihaloes

The emergence of the first generation of stars, known as Population III (Pop III) stars (Larson and Starrfield, 1971; Carr et al., 1984; Bromm, 2013), represents a pivotal point in cosmic history. These stars are theorized to have formed from pristine, metal-free gas via molecular hydrogen cooling (Haiman et al., 1996), in stark contrast to the metal-enriched stellar populations observed today (Baraffe et al., 2001; Bromm and Larson, 2004; Ventura et al., 2025a). Due to the different cooling mechanisms available in the early Universe, Pop III stars are expected to have been predominantly massive ($> 10 M_{\odot}$) and short-lived (Klessen and Glover, 2023), although some simulations find lower-mass Pop III stars when including turbulence, magnetic fields and ionizing radiation feedback (Sharda and Menon, 2025; Sharda et al., 2025).

The first stars and the subsequent population of X-ray binaries had a profound impact on the Universe and the observable 21-cm signal, leaving potentially detectable signatures (Carr et al., 1984; Mirocha et al., 2018; Schauer et al., 2019; Mebane et al., 2020; Qin et al., 2020; Gessey-Jones et al., 2022; Ventura et al., 2023; Pochinda et al., 2024; Cruz et al., 2025; Gessey-Jones et al., 2025; Hegde and Furlanetto, 2025; Katz et al., 2025; Liu et al., 2025a; Ventura et al., 2025b; Wasserman et al., 2025). Pop III stars were the first sources of light enabling the WF coupling for the first time (subsection 2.1), thus making the cosmic dawn 21-cm signal observable against the CMB. The remnants of these massive Pop III stars, particularly the luminous high mass X-ray binaries (Sartorio et al., 2023), are predicted to have played a crucial role in the evolution of the 21-cm signal by ushering the Universe into the era of cosmic heating (subsection 2.2). Furthermore, the massive Pop III stars are efficient in producing ionizing radiation (e.g. Schaerer, 2002; Wasserman et al., 2025; Liu et al., 2025a) and the copious soft-UV emission from the Pop III stars in the Lyman-Werner bands is thought to destroy the H_2 molecules required to cool the pristine primordial gas, thus locally delaying or even inhibiting star formation (Haiman et al., 1996; Ahn et al., 2012) and resulting in enhanced fluctuations in the 21-cm signal (Holzbauer and Furlanetto, 2012; Fialkov et al., 2013). The first supernovae initiated the process of metal enrichment and the transition to enriched stellar populations (Pallottini et al., 2014; Ventura et al., 2025b). Another unique signature that can be imprinted in the 21-cm signal by star formation in minihalos is the enhanced acoustic oscillations in the cosmic dawn power spectrum due to the relative motion between dark matter and gas (see section 4.6 and Tseliakhovich and Hirata, 2010; Fialkov et al., 2013; Zhang et al., 2024, for more details). These fluctuations are modulated by Pop III star formation, can probe small-scale density fluctuations, and are sensitive to the nature of dark matter.

These signatures of the Pop III stars and their remnants in the 21-cm signal depend on the masses of the first stars (e.g. Mebane et al., 2020; Gessey-Jones et al., 2022, 2025; Liu et al., 2025a; Wasserman et al., 2025). While the global (sky-averaged) 21-cm signal provides insights into the average thermal and ionization history, the true wealth of information about Pop III stars and their mass distribution lies in the spatial fluctuations of the 21-cm signal. Different models for Pop III star formation, their initial mass function (IMF), and their X-ray emission efficiencies are predicted to leave distinct imprints on the 21-cm power spectrum (Qin et al., 2020; Gessey-Jones et al., 2022, 2025; Liu et al., 2025a; Wasserman et al., 2025). The Pop III IMF is strongly linked to the stellar emissivity in the Lyman band (Gessey-Jones et al., 2022), the ionizing properties of stars (Schaerer,

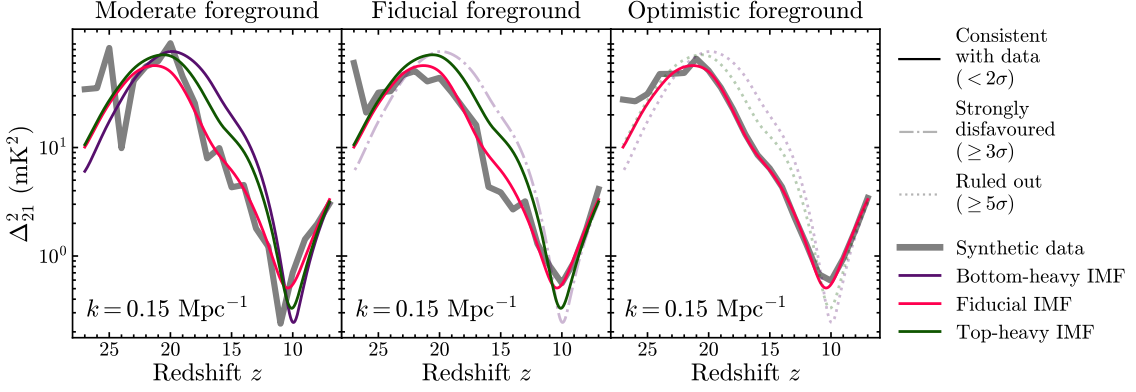


Figure 3: Forecasted Bayesian constraints on the Pop III IMF from the 21-cm power spectrum. We show the 21-cm power spectra simulated using the semi-numerical code 21cmSPACE for three candidate truncated power-law Pop III IMFs (different line colours), of the form $dN/dM \propto M^{-\alpha_{\text{IM}}}$, $M \in [M_{\text{min}}, M_{\text{max}}]$. Our bottom-heavy, fiducial and top-heavy IMFs correspond to the Sa1, Int-1 and Top IMFs considered in Gessey-Jones et al. (2025) respectively. The synthetic data are generated assuming a fixed fiducial IMF and noise levels simulated with 21cmSense for the full ‘AA4’ SKA antenna configuration with 10 MHz channel bandwidth and 3000 hours of observation, assuming three different foreground avoidance scenarios: ‘moderate’ (left), ‘fiducial’ (centre) and ‘optimistic’ (right). In the ‘optimistic’ scenario, only k-modes within the main lobe of the beam are excised. In the ‘fiducial’ scenario, we discard all k-modes within the horizon limit, and in the ‘moderate’ scenario an additional buffer of $0.1 h\text{Mpc}^{-1}$ above the horizon is removed. The line-style corresponds to the confidence with which each model is ruled out by the data, as summarized in the top right corner of the Figure.

2002; Liu et al., 2025a) as well as the average lifetime, abundance and luminosity of the subsequent XRB population (Sartorio et al., 2023). Thus, we expect the precise timing and intensity of features in the 21-cm power spectrum to be sensitive to the Pop III IMF across the wide redshift range observable by the SKA (Figure 3 and Gessey-Jones et al., 2025).

In Figure 3, we present the 21-cm power spectra at $k = 0.15 \text{ Mpc}^{-1}$ for three Pop III IMF types generated using the semi-numerical code 21cmSPACE⁴: a bottom-heavy case dominated by small-mass stars, a fiducial IMF, and a top-heavy IMF dominated by massive stars, (corresponding to the Sa1, Int-1, and Top IMFs considered in Gessey-Jones et al., 2025, respectively). The top-heavy case results in more efficient X-ray heating compared to the bottom-heavy case (Sartorio et al., 2023). This discrepancy leads to distinct power spectrum signatures in the 21-cm signal (Gessey-Jones et al., 2025), suggesting that models with strong Pop III X-ray emission are distinguishable from models with no or mild Pop III X-ray emission using 1,000 hours of foreground-avoidance observations with the upcoming SKA1-Low. However, as we learn from Figure 3, robust foreground treatment will likely be necessary to produce $3 - 5\sigma$ constraints on the IMF, with foreground avoidance alone being unlikely to yield constraints stronger than $\sim 2\sigma$. In Figure 3, we show the synthetic 21-cm data created using the fiducial IMF (following the procedure outlined in Section II of Gessey-Jones et al., 2025, but using updated noise levels simulated with 21cmSense). We then calculate the likelihood that the data are generated with a different IMF (bottom-heavy or top-heavy), assuming

⁴To create these curves, we fixed the remaining 21-cm model parameters, including Pop II physics, at the values specified in Table S.1 of Gessey-Jones et al. (2025).

three foreground avoidance scenarios: moderate, fiducial, and optimistic (see the caption of Figure 3 for details). We find that an aggressive foreground treatment is required to recover the true IMF at $> 3\sigma$ within 3,000 hours of observation.

The SKA-Low, with its unprecedented sensitivity across a wide range of redshifts, is uniquely positioned to measure subtle fluctuations driven by feedback from Pop III stars in minihaloes. The ability to simultaneously probe a range of scales and redshifts will be crucial for breaking degeneracies between different models of the first stars and their evolution. This will enable inference of elusive parameters such as the Pop III IMF, in the manner demonstrated with mock data in Fig. 3.

4.3 X-ray binaries

X-ray emission is another key ingredient of the early Universe, contributing to both the heating of the IGM and the ionization of the neutral hydrogen. Much remains uncertain: soft X-rays ($E \sim 20\text{eV}$) in the form of thermal emission from supernova remnants (Oh, 2001; Venkatesan et al., 2001; Ricotti and Ostriker, 2004) and mini-quasars (Kuhlen et al., 2006; Ciardi et al., 2010), hard X-rays ($E \sim 3\text{keV}$) from black hole X-ray binaries (XRBs; Mirabel et al., 2011; Fragos et al., 2013a), and AGN have all been suggested as dominant sources of X-ray emission. The properties of the X-ray background such as its strength, inhomogeneous heating effect (Pritchard and Furlanetto, 2007; Fialkov and Barkana, 2014), and shape of its spectral energy distribution (Fialkov et al., 2014; Fialkov and Barkana, 2014; Pacucci et al., 2014; Ross et al., 2017) affect the evolution of the IGM temperature, and thus the 21-cm signal coupled to it. The contribution of ancient X-ray sources to the unresolved X-ray background seen today sets an upper limit on their emission efficiency, and is thus a useful observable (Fialkov et al., 2017; Pochinda et al., 2024). X-rays also contribute to reionization, and can produce a fairly homogeneous low level of ionization. However, since heating gas to the CMB temperature requires far less energy than ionizing it, in most standard models the X-rays dominate early cosmic heating but ultra-violet photons dominate cosmic reionization.

XRBs are thought to be the most likely dominant source of X-ray emissions at $z \gtrsim 6$, in particular high-mass X-ray binaries (Fragos et al., 2013b; Lehmer et al., 2016). A simple model for their X-ray luminosity, following local starburst-like galaxies, assumes proportionality to the halo star-formation rate (e.g., Grimm et al., 2003; Lehmer et al., 2010; Mineo et al., 2012, 2014):

$$L_X/\text{SFR} = f_X \times 3 \times 10^{40} \text{ erg s}^{-1} \text{ M}_\odot^{-1} \text{ yr} , \quad (5)$$

where f_X is the X-ray emission efficiency of sources at high-redshifts, normalized to low redshift low metallicity X-ray binaries (Fragos et al., 2013a,b; Lehmer et al., 2021; Fialkov et al., 2017).

Given the weak current observational constraints on high-redshift X-ray sources, particularly on any temporary high-redshift population that may have had different properties than those of observed sources at lower redshifts, the X-ray efficiency is typically the dominant astrophysical uncertainty in standard astrophysical models of the 21-cm signal. This parameter may vary by up to several orders of magnitude below or above the “standard” value of unity, in turn making the predictions of the 21-cm power spectrum vary by several orders of magnitude. Low X-ray efficiency gives late X-ray heating, allowing the early IGM more time to cool adiabatically, producing stronger

21-cm absorption and extending this strong signal to lower redshifts. Thus, among standard astrophysical models, these yield the strongest 21-cm fluctuations and are the first models to be potentially detectable. Models with $f_X = 0$ are already strongly disfavoured or ruled out (e.g., HERA Collaboration et al., 2023), although this corner of the parameter space is particularly sensitive to weak heating sources, in particular Ly α heating (e.g., Chen and Miralda-Escudé, 2004; Chuzhoy and Shapiro, 2007; Mittal and Kulkarni, 2020; Reis et al., 2021) [Note that CMB heating is thought to be negligible (Venumadhav et al., 2018; Meiksin, 2021)]. As long as f_X is not too high, the hard X-ray spectrum expected for XRBs could produce a late heating during cosmic reionization, leading to a variety of signatures that should be observable with the SKA (Fialkov et al., 2014; Fialkov and Barkana, 2014; Pacucci et al., 2014; Ross et al., 2017; Watkinson et al., 2019).

In summary, an SKA detection of the 21-cm power spectrum during cosmic dawn will strongly constrain the intensity and spectrum of X-ray heating sources, at redshifts for which there are almost no other observational constraints. The redshift evolution of X-ray heating will help us determine if it is consistent with XRBs as the primary source.

4.4 Cosmic rays

While it has been extensively proposed that X-ray photons emitted by the earliest accreting black holes play the dominant role in heating the IGM during cosmic dawn and epoch of reionization, there are alternative heating mechanisms, such as, cosmic ray heating (Schlickeiser, 2002) that can complement or even compete with traditional X-ray heating, especially during early phases of cosmic dawn (Sazonov and Sunyaev, 2015; Leite et al., 2017; Jana et al., 2019; Bera et al., 2023; Gessey-Jones et al., 2023). The remnants of energetic supernovae (SNe), which mark the endpoints of massive Population III stars and Population II stars, could expand beyond their host dark matter minihalos into the surrounding IGM (Whalen et al., 2008), aided by the prior photoevaporation of halo's gas (Shapiro et al., 2004; Whalen et al., 2004), triggered by ultraviolet radiation from the progenitor star. It is argued that, during the evolution of such SN remnants, a considerable fraction of the kinetic energy could have been transferred into cosmic rays, which would eventually escape into the IGM (Hillas, 2005; Caprioli and Spitkovsky, 2014). Cosmic rays are considered to be generated in the termination shock of the supernova explosions originated from both Population III and Population II stars. As a significant fraction of supernovae kinetic energy gets injected into the cosmic rays, they are potential sources of heating of the IGM, and play a significant role in shaping the global 21-cm signal (Bera et al., 2023) and the 21-cm power spectrum (Gessey-Jones et al., 2023) during cosmic dawn. For instance, these sub-relativistic particles are expected to have propagated over large distances and deposited their energy into the IGM, leading to heating by $\sim 10 - 100$ K by redshift $z \sim 15$, prior to the onset of more dominant heating and ionization processes driven by the first galaxies and quasars. Cosmic rays from young galaxies could also heat and ionize the IGM in the context of both the reionization and post-reionization epochs (Ginzburg and Ozernoi, 1966; Nath and Biermann, 1993; Samui et al., 2005, 2018). Additionally, cosmic rays can originate not only from galaxies but also from microquasars and can have an impact on reionization (Turoes et al., 2014).

The low-energy cosmic rays from Pop III stars can escape their host dark matter minihalos and

efficiently deposit energy into the IGM through Coulomb interactions and ionizations (Stacy and Bromm, 2007; Sazonov and Sunyaev, 2015). In contrast, high-energy cosmic rays from Pop II stars heat the IGM indirectly through the damping of magnetosonic Alfvén waves, and their effect becomes more prominent at lower redshifts (Samui et al., 2018). Depending on the efficiencies of cosmic ray production, the heating can significantly modify the shape and depth of the global 21-cm absorption signal (Bera et al., 2023). Moreover, when combined with scenarios involving dark matter-baryon interactions, which can cool the IGM and produce the unusually deep absorption feature (Barkana, 2018a; Muñoz and Loeb, 2018), cosmic ray heating can provide sufficient energy to raise the IGM temperature above that of the CMB effectively. The spectral shape of the global 21-cm signal is sensitive to CR parameters, such as acceleration efficiency and spectral slope, offering a new window into constraining early star formation and feedback processes (Bera et al., 2023).

Not only the global signal, cosmic rays from early galaxies can significantly affect the fluctuations and morphology of the 21-cm signal (e.g. Jana and Nath, 2018; Gessey-Jones et al., 2023). The cosmic ray heating introduces a smoother and more spatially extended heating profile compared to soft X-rays, as these particles travel further from their sources before depositing energy. This extended heating leads to a suppression of small-scale power in the 21-cm power spectrum during cosmic dawn, especially at redshifts $z \sim 15 - 20$. Depending on the energy injection efficiency and propagation properties, the peak of the 21-cm power spectrum may shift to lower redshifts, and its amplitude can be significantly reduced compared to standard X-ray-dominated scenarios (Gessey-Jones et al., 2023). These signatures offer a distinct observable imprint of cosmic ray heating that can be tested with SKA-Low.

On the other hand, in tomographic images of the 21-cm brightness temperature, the presence of cosmic ray heating results in more diffuse and gradual temperature transitions, unlike the sharp contrast between cold and heated regions seen with localized X-ray sources (Gessey-Jones et al., 2023). This smooth temperature distribution can erase the clear bubbles of heating typical of early galaxies, replacing them with large, mildly heated regions. As a result, tomographic maps show a reduced patchiness in brightness temperature and a more uniform heating morphology at high redshifts. Therefore the inclusion of cosmic ray heating not only delays the onset of 21-cm fluctuations but also modifies the spatial structure of the signal, making it a key observable targeting the epoch of reionization and cosmic dawn.

The SKA-Low will enable high-precision studies of cosmic rays in the energy range $\sim 10^{16} - 10^{18}$ eV, covering the transition between the Galactic and extragalactic regimes. The dense SKA-Low core, comprising $\sim 6 \times 10^4$ antennas within a ~ 1 km² area, will allow detailed radio detection of extensive air showers initiated by high-energy cosmic rays (Huege et al., 2017; Buitink et al., 2016; Schröder, 2017). Simulations indicate that SKA can achieve a depth of shower maximum measurement precision of $\sigma(X_{\max}) \simeq 6$ g cm⁻² for $\sim 10^{17}$ eV showers, significantly surpassing current radio arrays such as LOFAR (Schellart et al., 2013).

4.5 Supermassive black holes

Until now several hundred quasars have been discovered before the end of reionization (Bosman, 2020), among them, one has the highest redshift of ~ 10.1 (Natarajan et al., 2024), approaching the Cosmic Dawn. These quasars are powered by supermassive black holes (SMBHs) with typical masses $\sim 10^7 - 10^{10} M_\odot$ (Takahashi et al., 2024). On the other hand, JWST has identified several hundred Little Red Dots (LRDs) above redshift ~ 5 (Matthee et al., 2024). They are believed to be AGNs powered by SMBHs with masses below $\sim 10^7 M_\odot$ (Rusakov et al., 2025). Spectroscopically confirmed SMBHs have a number density $\sim 10^{-4} \text{ Mpc}^{-3}$ at $z \sim 6$ (Harikane et al., 2023), while an estimation based on photometric variability is as high as $\sim 10^{-2} \text{ Mpc}^{-3}$ (Hayes et al., 2024; Cammelli et al., 2025). These high redshift SMBHs have large uncertainties regarding their seeds, number density, and properties, all of which can differ significantly from low redshift ones, and could potentially be constrained from their imprints on the 21-cm signals. In particular, high redshift SMBHs appear overmassive relative to their hosts, with black hole mass to stellar mass ratios, M_\bullet/M_* , of $\sim 0.01 - 0.3$, sometimes approaching unity – far above the local value of ~ 0.001 (Maiolino et al., 2024).

The origin of the SMBH seeds and their growth is a long-standing puzzle. Three popular astrophysical scenarios have been proposed (Volonteri, 2010): light seed, medium seed and heavy seed. The most natural one is the stellar mass black holes ($\sim 10^2 M_\odot$) from Pop III star remnants (Heger and Woosley, 2002), which is the light seed scenario. Runaway collisions of stars in extremely dense stellar clusters may yield heavier seeds ($\sim 10^2 - 10^3 M_\odot$), and this is the medium seed scenario. Additionally, seeds as massive as $\sim 10^4 - 10^6 M_\odot$ can form from the collapse of pristine metal free gas in atomic-cooling halos where H_2 cooling is suppressed (Begelman et al., 2006), and this is the heavy seed scenario. In this scenario, the gas either collapses into a black hole directly, or experiences a short main sequence phase of a supermassive star with a comparable mass before that. They are all classified as direct collapse black holes (DCBHs). The light seed scenario demands nearly continuous Eddington or super-Eddington accretion, which is difficult to sustain (Alvarez et al., 2009), while in the medium seed scenario the collapse could only happen under rare, extremely dense conditions. For this reason, DCBHs are considered to be a promising scenario, as they naturally produce the overmassive black holes with accretion rate close to or even exceeding the Eddington limit (Pacucci and Ferrara, 2015). Dynamical heating (Wise et al., 2019) or radiation from other previously-formed DCBHs (Yue et al., 2017) may promote their formation and boost the abundance to above the observed number density level of SMBHs. Moreover, a DCBH has a higher chance to be observed directly, due to its large mass and high accretion rate.

Until now, DCBHs have not been identified in observations. Their number density is constrained by the observed high- z AGNs, since each AGN at least has one seed. Thanks to the special formation process, DCBHs are believed to be Compton-thick at birth, and their ionizing and soft X-ray photons are heavily absorbed. Their direct contribution to reionization is negligible, but may still essentially change the thermal history of the IGM and hence the 21-cm signal. The predicted influence on the 21-cm power spectrum is shown in left panel of Fig. 4, in comparison with the uncertainties of the SKA-low AA*. Note that the uncertainties at the large-scale end are dominated by the residual foregrounds, and the uncertainties at the small-scale end are mainly due to thermal noise and the

limited number of long baselines.

In addition to the DCBHs in Cosmic Dawn, the SMBHs will also imprint distinctive features on the 21-cm signals during the EoR. Compared with regular star-forming galaxies, SMBHs are rarer and more biased, and they can generate giant ionized bubbles around them. Inside these bubbles, the gas is fully ionized and there is no 21-cm signal. At the edge of the ionized bubble, the gas is heated and partially ionized, which produces a strong emission signal. Well beyond the edge, the 21-cm signal approaches the level of the mean IGM, which is weak emission during the EoR. According to recent observations carried by JWST, the number density of the high- z SMBHs could be $\gtrsim 10^{-4} \text{Mpc}^{-3}$ (Harikane et al., 2023), and $M_{\bullet}/M_{*} \gtrsim 0.01$ (Maiolino et al., 2024). The brighter SMBHs and their giant ionized bubbles are suitable for detection as individual targets. However, based on the SMBHs growth scenario, it is quite possible that there are more fainter SMBHs below the detection limit and/or at higher redshifts, and could be potentially more promising to be detected from their imprints on 21-cm signals. A typical 21-cm observation may have a survey volume $\gtrsim 10^6 - 10^7 \text{Mpc}^{-3}$, there must be numerous SMBHs in the volume. It is challenging to directly image the ionized bubbles around them, however, biased ionized bubbles can influence the statistics of the 21-cm signal, so 21-cm observations can provide information of the SMBHs as well.

The right panel of Fig. 4 show the predicted influence of SMBHs on the 21-cm power spectrum, compared with the observational uncertainties for SKA-low AA*. Indeed, in the presence of SMBHs, the 21-cm signal becomes more anisotropic on large scales, and has a lower power on intermediate scales. The feature on intermediate scales is larger than the uncertainties of SKA-low AA*, so the telescope has the potential to detect the SMBHs via 21-cm power spectrum. On large scales, the feature is buried in the foreground because if a moderate foreground removal model is adopted. However, in the case of optimistic foreground removal model, the uncertainties would be subdominant, and larger-scale 21-cm power spectrum could also help distinguish features induced by SMBHs.

In summary, DCBHs mainly influence the 21-cm power spectrum at Cosmic Dawn by almost uniformly heating the IGM with hard X-rays, while SMBHs mainly influence the 21-cm power spectrum at the EoR, when the IGM is already heated to $\gg T_{\text{CMB}}$, by generating giant biased ionized bubbles. Moreover, a SMBH also has the chance to be observed directly by the SKA if it is in the radio-loud phase. For a SMBH with mass $\sim 10^8 M_{\odot}$ and accretion rate 1% of the Eddington limit, if it is located at redshift 7 and has a radio luminosity following the relation of radio-loud samples in Bariuan et al. (2022), then its flux would be of the order of 1000 mJy at 200 MHz. This is well above the noise level of SKA-low AA* with 1 MHz bandwidth and 10 hour integration time.

4.6 Velocity acoustic oscillations

While regular baryonic matter interacts with radiation, most of the likely candidates for dark matter particles do not. At recombination, this imparts different initial conditions to these two fluids, manifesting as a streaming relative velocity between them. In Tseliakhovich and Hirata (2010) it was shown that this relative velocity is supersonic after baryon-photon decoupling (given the relatively low sound speed of baryons post-recombination), and remains so until the baryonic gas

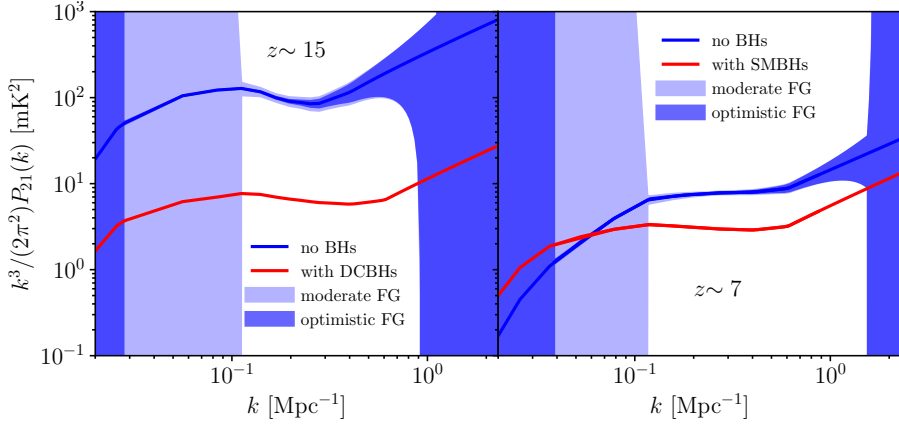


Figure 4: *Left:* The 21-cm power spectrum in Cosmic Dawn, in the absence/presence of DCBHs. DCBHs abundance is normalized to $\sim 10^{-2} \text{ Mpc}^{-3}$ at $z \sim 10$. *Right:* The 21-cm power spectrum in EoR, in the absence/presence of SMBHs. The SMBHs number density is normalized to be $\sim 2 \times 10^{-3} \text{ Mpc}^{-3}$ at $z \sim 6$. In all panels the filled regions refer to the SKA-low AA* uncertainties with $t_{\text{obs}} = 1080 \text{ hr}$ and a bandwidth of 10 MHz. The uncertainties are calculated by using 21cmSense, and optimistic (darker) and moderate (lighter) foreground removal models are assumed.

is heated by the first luminous sources. As a consequence, this relative velocity strongly modulates the star-formation rate density, chiefly through three effects: it suppresses the amount of structures formed (Tseliakhovich and Hirata, 2010; Naoz et al., 2012; Bovy and Dvorkin, 2013), their gas content (Tseliakhovich et al., 2011; Dalal et al., 2010; Naoz et al., 2013), and the star-formation rates in those structures (Greif et al., 2011; Stacy et al., 2011; O’Leary and McQuinn, 2012; Fialkov et al., 2012; Hirano et al., 2018; Schauer et al., 2021; Hegde and Furlanetto, 2023; Conaboy et al., 2023; Ventura et al., 2023, 2025b). Regions of large relative velocity will form fewer stars, and in turn their 21-cm signal will be delayed when compared to low-velocity regions, which has now been demonstrated in both semi-numerical models (Fialkov et al., 2012) and full simulations (Ahn, 2016; Conaboy et al., 2023).

The 21-cm maps observed by the SKA will inherit the fluctuations of the dark-matter—baryon velocity imprinted at recombination, which show up as “wiggles” on the 21-cm power spectrum (Dalal et al., 2010; Visbal et al., 2012; Fialkov et al., 2013; Muñoz, 2019; Conaboy et al., 2023; Cruz et al., 2025). These wiggles are termed velocity acoustic oscillations (VAOs) and provide a new standard ruler to measure cosmology with the SKA at high redshifts (Muñoz, 2019). The VAOs have a different shape than the low-redshift density BAOs (e.g., Eisenstein and Hu (1998)), but the same acoustic origin. Fig. 5 shows a plot of the 21-cm power spectrum with and without relative velocities at different redshifts. While the power spectra with no streaming velocities exhibit acoustic oscillations on the order of $\sim 5\%$ from the baseline, adding relative velocity fluctuations yields much more pronounced $\mathcal{O}(1)$ oscillations with peaks shifted from the no- v_{cb} case. The position of these VAO peaks are sensitive to the cosmic expansion and geometry at previously uncharted cosmic epochs. Their applications include measuring the Hubble expansion rate at $z = 10 - 20$ (Muñoz, 2019; Sarkar and Kovetz, 2023), searching for inflationary isocurvature modes (Hotinli et al., 2021), testing beyond-concordance cosmological models such as fuzzy dark matter (Sarkar et al., 2022;

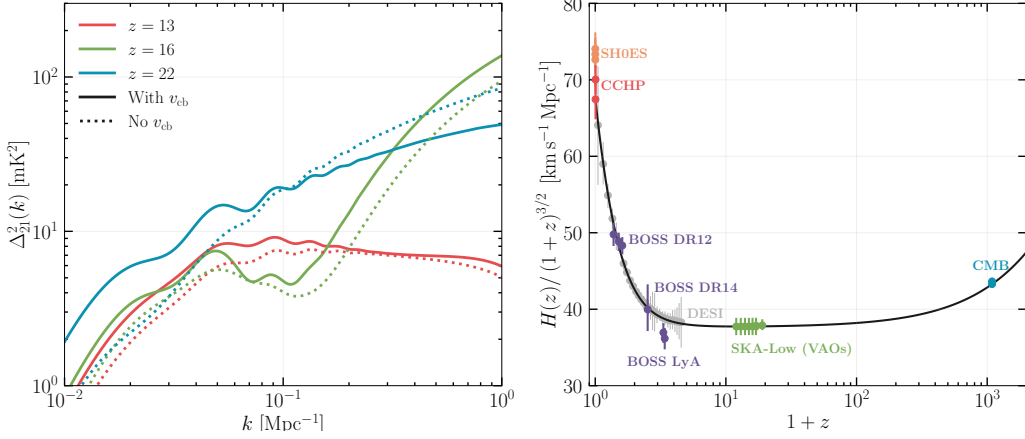


Figure 5: A depiction of how velocity-induced acoustic oscillations (VAOs) can be used to measure cosmic expansion. *Left:* The 21-cm power spectrum at $z = 13, 16, 22$ computed with Zeus21 (Muñoz, 2023; Cruz et al., 2025) in the absence (dotted) and presence (solid) of dark matter-baryon relative velocities v_{cb} . Including the streaming effects alter the spectral shape, leading to more pronounced acoustic features whose peaks measure the quantity $H(z)r_s$. *Right:* Existing measurements of the Hubble parameter $H(z)$ across cosmic time with different probes, along with forecasted constraints from future 21-cm experiments. Namely, we plot the constraints from the CMB (Louis et al., 2025; Planck Collaboration et al., 2020) (blue), from forecasts of future SKA-Low observations (Muñoz, 2019; Sarkar and Kovetz, 2023), galaxy clustering measurements with BOSS (Alam et al., 2017; Zarrouk et al., 2018; Bautista et al., 2017) (violet) and DESI (DESI Collaboration et al., 2016; Adame et al., 2025; Abdul Karim et al., 2025) (gray), from type Ia supernovae (Riess et al., 2019, 2022, 2024) (orange), and tRGB measurements (Freedman et al., 2025; Lee et al., 2025) (red).

Flitter and Kovetz, 2022; Hotinli et al., 2022), primordial magnetic fields (Sethi and Subramanian, 2005; Tashiro and Sugiyama, 2006; Schleicher et al., 2008, 2009; Bowman et al., 2018; Kunze, 2019; Minoda et al., 2019; Cruz et al., 2024; Bhaumik et al., 2025), new light degrees of freedom (e.g. light neutrino-like species (Montefalcone et al., 2025)), and models where dark matter interacts with baryons (Muñoz and Loeb, 2018; Sun et al., 2025a; Rahimieh et al., 2025; Liu et al., 2019).

Observationally, the SKA is well positioned to observe VAOs. VAOs always enhance the 21-cm power spectrum, and the presence of relative velocities pushes the signal to lower z (all parameters being equal), both of which aid in detection. Separating VAOs from the smooth signal, however, requires relatively good k resolution, for which baseline and bandwidth distribution are important. A promising technique is in the form of AI-inspired techniques such as wedge reconstruction (Kennedy et al., 2024; Sabti et al., 2025), which are expected to thrive in the large volumes observed by the SKA. VAOs are most prominent during cosmic dawn when halo masses are lower, and therefore are more susceptible to the suppressive effects of the velocity differential. However, it may be possible to observe VAOs and its relics towards lower redshifts. Small-scale clumping in the IGM eventually become important photon “sinks” during reionization but may be subject to pressure smoothing effects from the streaming velocity. Such an effect could impact the ionizing efficiency of early galaxies and the large-scale variation in reionization history (Cain et al., 2020; Park et al., 2021).

4.7 Other standard signatures

In this section we briefly summarize a few other 21-cm signatures that are expected in the standard Λ CDM model: small-scale clumping, line-of-sight anisotropy, and 21-cm polarization.

In standard CDM, small-scale clumping is predicted to affect the 21-cm signal. At high redshifts, when star formation is still rare, dense dark matter clumps form due to structure formation and pull in gas that is then heated. Due to the non-linearity of these fluctuations, they do not average out, but change the 21-cm signal as seen on much larger scales (Ahn et al., 2006; Shapiro et al., 2006; Ali-Haïmoud et al., 2014; Xu et al., 2018; Cain et al., 2020; Bianco et al., 2021; Xu et al., 2021; Park et al., 2025). In particular, clumping has a strong impact on the large-scale 21-cm power spectrum (Bianco et al., 2021; Sikder et al., 2025); after the Dark Ages, once Ly α coupling kicks in due to the first stars, the 21-cm signal strengthens, and clumping suppresses the observable power spectrum around redshift 20 by as much as a factor of two. As the clumping effect arises from small-scale density fluctuations (typical mass scale of 20 million solar masses), it offers a unique opportunity to probe the standard cold dark matter model in a new regime and thus potentially investigate the properties of dark matter, adding new constraint to models such as warm dark matter and fuzzy dark matter (Hu et al., 2000). The clumping effect in CDM is significantly higher than the sensitivity of the planned SKA AA* configuration, by up to a factor of 20, though detection will require separation from foregrounds and from astrophysical contributions to the 21-cm power spectrum. It may also be possible to constrain similar scales through their effect on the formation of small halos and the 21-cm effect of astrophysical radiation from those halos (Muñoz et al., 2020).

While most 21-cm analyses in anticipation of the SKA focus on the spherically-averaged 21-cm power spectrum, a significant line-of-sight anisotropy is expected in the standard case, potentially enabling more information to be extracted. Gas motions along the line of sight produce an anisotropy due to the line-of-sight velocity gradient (Barkana and Loeb, 2005a) that arises through the Kaiser effect of redshift-space clustering (Kaiser, 1987; Bharadwaj and Ali, 2004). For linear fluctuations, this dependence on the angle to the line of sight makes it possible to measure three separate coefficients (Barkana and Loeb, 2005a), corresponding to the power spectrum of density fluctuations, the power spectrum of isotropic 21-cm fluctuations, and their cross-correlation. Numerical investigations during cosmic reionization (McQuinn et al., 2006; Mao et al., 2012; Jensen et al., 2013; Shapiro et al., 2013) suggest that the decomposition of the line-of-sight anisotropy is more complex than the simple linear limit, but it should still provide additional information that will help track the evolution of 21-cm fluctuations over various eras (Fialkov et al., 2015). An additional source of 21-cm anisotropy is the light-cone anisotropy (Barkana and Loeb, 2006); the look-back time changes with the radial distance, and the character of the 21-cm fluctuation sources evolves with time, which results in a line-of-sight effect that introduces anisotropy. In particular, this can generate a significant anisotropy on large scales near the end of reionization, as has been studied in numerical simulations (Datta et al., 2012, 2014; La Plante et al., 2014; Zawada et al., 2014). Also, if 21-cm data are analyzed using assumed cosmological parameters that differ from the true ones, this causes an Alcock-Paczynski (Alcock and Paczynski, 1979) anisotropy that can be used to constrain cosmological parameters (Ali et al., 2005; Nusser, 2005) through an additional anisotropic term added (in the limit of linear fluctuations) to the 21-cm power spectrum (Barkana, 2006). Some

exotic models can produce a strong line-of-sight anisotropy (e.g., see Sec. 5.1). It remains to be seen to what degree the SKA can measure the signal’s intrinsic line-of-sight anisotropy, given that the anisotropy is a fundamental part of algorithms for removing and/or avoiding the strong foreground.

While most studies of high-redshift 21-cm signatures focus on the total intensity (Stokes I) of the 21-cm signal, its polarization (Stokes Q , U and V) presents a complementary window into CD/EoR. In addition, Faraday rotation of the linear polarization signals offers a possible synergy between Cosmic Dawn and the cosmic magnetism science goals of SKA (Johnston-Hollitt et al., 2015; Heald et al., 2020). The dominant mechanism for generating the 21-cm polarization signal is Thomson scattering of the 21-cm photons off free electrons in the ionized IGM (Babich and Loeb, 2005). Analogous to the CMB polarization, this process converts the quadrupole moment of the primary 21-cm temperature field into linear polarization, predominantly of the E-mode type for scalar perturbations. Therefore, this signal is sourced by a much larger volume than that for the temperature signal (the latter is restricted to the past light cone), thus carrying unique information about the distribution and morphology of the ionized regions. A prediction for this signal was made by Li et al. (2021), using semi-numerical simulations that capture inhomogeneous reionization. The overall amplitude of the angular power spectrum was found to be weaker than the sensitivity of SKA1-Low, with the peak of the EE spectrum reaching only $\sim 1 \mu\text{K}$ and the TE spectrum $\sim 0.03 \text{ mK}$. Notably, the TE spectrum exhibits a distinctive zero-crossing at large angular scales ($\ell < 100$) that is a potential new diagnostic of reionization physics. A major challenge to the detection of this E-mode polarization is Faraday rotation from Galactic magnetic fields (De and Tashiro, 2014), but cross-correlation approaches may enhance detectability (Ji et al., 2023). Circular polarization of the 21-cm radiation (Stokes V) can arise from the Zeeman effect due to intergalactic magnetic fields (Cooray and Furlanetto, 2005), as well as from the interaction between the spin-polarization quadrupole of neutral hydrogen atoms and the quadrupole anisotropy of the CMB, providing a potential probe of primordial gravitational waves (Hirata et al., 2018; Mishra and Hirata, 2018). The predicted signal in ΛCDM model peaks at $\ell \sim 400$ and $z \sim 17$ but is still orders of magnitude beyond detection by the SKA (Ji et al., 2021).

5 Exotic Signatures

In this section we summarise potential signatures from exotic sources and new physics beyond the ΛCDM framework.

5.1 Strongly-emitting radio galaxies

The Absolute Radiometer for Cosmology, Astrophysics, and Diffuse Emission (ARCADE-2, Fixsen et al., 2011) measurements at GHz frequencies revealed a strong radio background, significantly deviating from the CMB blackbody spectrum at low frequencies. This was corroborated by the first station of the Long Wavelength Array (LWA-1, Dowell and Taylor, 2018) in the 40 – 80 MHz range. The amplitude of this radiation exceeds the expectations based on known Galactic and extragalactic radio sources (Singal et al., 2018; Singal et al., 2023), making its origin an interesting astrophysical puzzle. Proposed explanations include exotic processes such as dark matter annihilation (Fraser et al., 2018; Pospelov et al., 2018), superconducting cosmic string (Brandenberger et al., 2019),

radiative decay of relic to sterile neutrinos (Chianese et al., 2019) in the early Universe or radio emission from accreting supermassive primordial black holes (Mittal and Kulkarni, 2022a). A more astrophysically grounded explanation of this observed radio excess could be a population of high-redshift radio galaxies (Condon et al., 2012). The Galactic contribution to the radio background is significantly uncertain (Subrahmanyan and Cowsik, 2013), but the observed background certainly puts an upper limit on the contribution from any extragalactic source population.

The tentative detection of an absorption profile by EDGES (Bowman et al., 2018) at ~ 78 MHz (corresponding to a redshift $z \sim 17$) along with the extragalactic radio background measured by ARCADE-2 have spurred significant interest in understanding excess radio emissions from astrophysical sources and their impact on the 21-cm signal. The enhancement of the CMB by an excess radio background, as an explanation for the EDGES experiment, was initially explored without focusing on particular sources (Bowman et al., 2018; Feng and Holder, 2018; Fialkov and Barkana, 2019). However, high-redshift galaxies are natural candidates for such a background

To investigate this possibility, Mirocha and Furlanetto (2019) modelled the radio emissivity as proportional to the star formation rate (SFR), as observed in present-day galaxies (Gürkan et al., 2018), and found that high-redshift galaxies would need to be approximately 1,000 times more radio-luminous than their present-day counterparts (relative to the SFR) to explain the EDGES signal (see also Mittal and Kulkarni (2022b)). We note that the SARAS measurement has presented counter-evidence to the EDGES results (Singh et al., 2022), while other analysis methods disfavour an excess radio background in relation to EDGES (Cang et al., 2025).

High-redshift galaxies should produce an inhomogeneous radio background due to their clustered distribution. Incorporating this into a 21-cm semi-numerical code, Reis et al. (2020) showed that this inhomogeneity introduces a new type of fluctuations in the 21-cm signal. Since the 21-cm absorption occurs along the line of sight, it is therefore sensitive to radio sources lying behind each absorbing cloud. Including this line-of-sight effect (Sikder et al., 2024b) enhances the 21-cm power spectrum during cosmic dawn, by up to two orders of magnitude. This also induces a new anisotropy in the 21-cm power spectrum. Note that in these models, during the late stages of reionization the radio fluctuations disappear due to the rising abundance of radio sources.

As noted above, the intensity of the observed extragalactic radio background puts an upper limit on the excess radio emission from high-redshift sources. Additional constraints are placed by the observational upper limits on the clustering of the radio background. In particular, there are measured limits on arcminute-scale anisotropy from the Very Large Array at 4.9 GHz (Fomalont et al., 1988) and the Australia Telescope Compact Array at 8.7 GHz (Subrahmanyan et al., 2000). These provide the strongest current constraints on radio emission by high-redshift galaxies (Holder, 2014; Sikder et al., 2024a), although models are still allowed that are consistent with EDGES.

Figure 6 shows the maximum 21-cm power spectrum from models with strongly-emitting radio galaxies, given current observational constraints (Sikder et al., 2024a) on radio galaxy populations from various redshifts. Populations with high radio efficiencies may have existed only at high redshifts. The maximum power spectrum is 6×10^6 mK² (from $z = 16$) given the constraint on the intensity of the observed extragalactic radio background, lowered to 1.3×10^5 mK² (from $z = 19$)

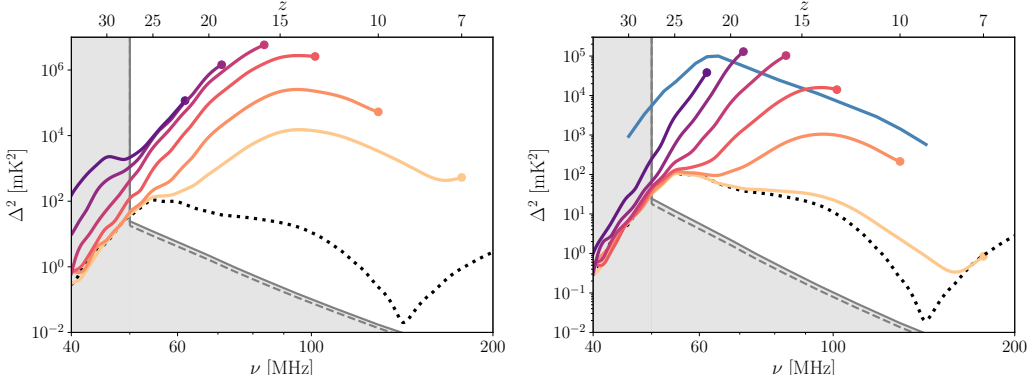


Figure 6: An estimate of the maximum 21-cm power spectrum from models with strongly-emitting radio galaxies, given current observational constraints (based on Fig. 5 of Sikder et al. (2024a)). We show the power spectrum (in terms of the squared fluctuation in mK^2) at wavenumber $k = 0.1 \text{ Mpc}^{-1}$, versus observed frequency ν and redshift z . Each coloured curve that ends with a dot shows the prediction of a particular model with a fixed radio-emission efficiency, compared to observational constraints assuming that the corresponding galaxy population persisted down to the redshift where the curve ends. **The upper envelope of all these curves should be seen as the prediction.** The ending redshifts are 7, 10, 13, 16, 19, and 22. We also show for comparison the case with no excess radio background, i.e., with the CMB as the assumed background (dotted black line). Also shown is the $k = 0.1 \text{ Mpc}^{-1}$ sensitivity for the SKA configuration AA* (solid grey line and the corresponding shaded area) and configuration AA4 (dashed grey line); this shows thermal noise, assuming 1080 hours of total integration time and optimistic foreground removal, using the code 21cmSense (Pober et al., 2013, 2014). *Left:* Includes the constraint on the intensity of the observed extragalactic radio background. *Right:* Includes also the observational upper limits on the clustering of the radio background. Separately, we show (solid blue curve) an estimate of the maximum power spectrum from a model with a baryon – dark matter interaction (Sec. 5.3), from Fig. 1 of Barkana et al. (2023), for the interacting millicharged dark matter model at wavenumber $k = 0.13 \text{ Mpc}^{-1}$.

once we include the observational upper limits on the clustering of the radio background. The latter is still more than 3 orders of magnitude higher than the power spectrum of the same model in its standard version, without an excess radio background. It is 5 orders of magnitude above the expected SKA sensitivity.

5.2 Primordial magnetic fields

Magnetic fields exist everywhere in the universe (Govoni and Feretti, 2004; Durrer and Neronov, 2013). The origin of these cosmic magnetic fields is under discussion, and a possible scenario is that a tiny magnetic field is generated in the early universe, which is called “Primordial magnetic fields (PMFs)”, and they evolved to be the galactic and/or intergalactic magnetic fields (for a recent review of the PMF scenario, for instance, see Subramanian 2016). Note that the astrophysical processes may also produce large-scale magnetic fields in the late universe (Biermann, 1950; Pouquet et al., 1976; Brandenburg and Subramanian, 2005). In particular, observations of magnetic fields on large scales, such as in void regions or large-scale structure, may invoke generation scenarios in the early universe (Ando and Kusenko, 2010; Neronov and Vovk, 2010).

PMFs induce small-scale IGM gas perturbations through Lorentz forces on the baryon fluid, in addition to the standard curvature perturbations (Wasserman, 1978; Kim et al., 1996). Unlike

standard ones, PMFs induce isocurvature-like fluctuations that are inherently non-Gaussian and strongly scale-dependent. These PMF-induced fluctuations can dominate the small-scale power spectrum, especially below the magnetic Jeans scale, and the field strength and scale dependence of PMFs determine the characteristic scale of the induced fluctuations. Consequently, PMFs can amplify structure formation seeds by increasing density fluctuations at high redshifts.

PMFs induce not only density fluctuations, but also the IGM gas temperature fluctuations at high redshifts. There are two main processes by which PMFs heat up IGM gas: ambipolar diffusion and MHD turbulence after recombination. The former is brought by Coulomb scattering acting between neutral and ionized particles in a partially ionized plasma, and the latter is a nonlinear energy cascade process from large-scale eddies to small-scale ones. Sethi and Subramanian (2005) has calculated the IGM thermal history including these processes, and they have shown that IGM gas temperature is increased up to $\sim 10^4$ K with nano-Gauss PMFs.

The 21-cm signal is a promising tool for probing baryon gas density and temperature at high redshifts. Considering the above effects of PMFs on the IGM gas physics, Schleicher et al. (2008, 2009) have predicted the 21-cm signal with PMFs. Minoda et al. (2019) has taken into account the decrease in energy of PMFs and put a constraint on PMF strength from the measurement of the 21-cm global signal with *EDGES* (Bowman et al., 2018). Future experiments of the 21-cm global signal may improve understanding of PMFs.

On the other hand, in a colder IGM enabled by dark matter-baryon interactions (Barkana, 2018a; Muñoz and Loeb, 2018), the residual free electron fraction and Compton coupling are both suppressed (Datta et al., 2020). These effects significantly enhance the PMF-induced heating rates (via ambipolar diffusion and decaying turbulence) compared to the standard cosmological scenario (Sethi and Subramanian, 2005; Chluba et al., 2015; Minoda et al., 2019; Bera et al., 2020). Consequently, even relatively weak PMFs (with present-day strength $B_0 \lesssim 0.5nG$) can transfer a substantial fraction of their magnetic energy into heating the IGM. This rapid energy transfer causes the PMF to decay faster than the conventional $(1+z)^2$ scaling during the dark ages and cosmic dawn, indicating that PMFs are unlikely to be the primary cause of the later heating require to raise the temperature above CMB, though they shape early thermal history (Bera et al., 2020; Minoda et al., 2019).

Moreover, when dark matter-baryon interactions and PMFs act together, a plateau-like feature appears in the redshift evolution of the IGM temperature because of the interplay between cooling from DM-baryon scattering and the PMF heating over a range of $z \sim 50-150$ (Bera et al., 2020). Importantly, the upper limits on allowed B_0 depend sensitively on the DM interaction strength σ and DM particle mass m_χ . While PMFs stronger than ~ 0.1 nG are disallowed in standard models without DM-baryon scattering (Minoda et al., 2019), values up to ~ 0.4 nG become permissible if DM-baryon scattering is effective (for suitable combinations of m_χ and σ) (Bera et al., 2020). However, PMFs $\gtrsim 1$ nG remain unlikely, as they would require unrealistically strong cooling to offset the magnetic heating. Thus, the joint effects of PMFs and DM-baryon interactions significantly alter PMF evolution and the resulting IGM temperature history, with strong implications for interpreting the global 21-cm signal (Minoda et al., 2019; Bera et al., 2020; Bhaumik et al., 2025).

Not only is the global signal of the 21-cm line from the cosmic dawn affected by PMFs, but the 21-cm power spectrum is also affected (Sethi and Subramanian, 2005; Tashiro and Sugiyama, 2006; Schleicher et al., 2009; Kunze, 2019). Since both the matter fluctuations and the temperature fluctuations affect the inhomogeneous 21-cm signal, their contributions are highly nonlinear effects. Therefore, predicting the PMF constraint from the 21-cm power spectrum needs careful discussion. The 21-cm power spectrum from the pre-reionization era with SKA might improve bounds on the PMFs $\lesssim 0.01 - 0.1$ nG (Cruz et al., 2024; Bhaumik et al., 2025).

5.3 Baryon – Dark Matter Interactions

A number of exotic physical models were stimulated by the possible EDGES detection of a strong 21-cm signal during cosmic dawn (Bowman et al., 2018). While disputed at 95% significance by the SARAS experiment (Singh et al., 2022), with further measurements expected to resolve this tension, the tentative EDGES signal has inspired theories that can be probed over a wide range of possible parameters, independently of whether EDGES turns out to be correct.

One category of explanations for EDGES is the combination of Ly α coupling from early galaxies with a mechanism that cooled the gas faster than just adiabatic cooling due to the cosmic expansion (Barkana, 2018b). The additional cooling mechanism that was suggested (Dvorkin et al., 2014; Tashiro et al., 2014; Muñoz et al., 2015; Muñoz and Loeb, 2017) involves a non-gravitational interaction between the ordinary matter and the dark matter particles (e.g., via Rutherford-like scattering); this drives down the gas temperature, leading to the strong observed absorption.

Any particle physics model that supplies such a new scattering interaction faces additional constraints (Berlin et al., 2018; Barkana et al., 2018), including those on dark matter self-interaction (constrained by the known distribution of dark matter around galaxies) as well as baryon self-interaction, i.e., a fifth force (constrained by laboratory measurements). A model that satisfies these constraints is millicharged dark matter, in which a small fraction of the dark matter particles have a tiny electric charge, and Coulomb scattering is responsible for the energy transfer (Muñoz and Loeb, 2018; Muñoz et al., 2018). With any baryon – dark matter interaction, the strong correlation between baryon temperature and the baryon – dark matter relative streaming velocity (Tseliakhovich and Hirata, 2010) tends to imprint large velocity acoustic oscillations on the 21-cm signal (Barkana, 2018b). However, this signature is erased in the millicharged dark matter model by drag at early times, throughout the viable parameter space of this model (Kovetz et al., 2018). It is possible to restore this signature in an interacting millicharged dark matter model (Liu et al., 2019; Barkana et al., 2023), which is more elaborate (adding a long-range interaction between the millicharged part and the rest of the dark matter) but also is viable over a much wider range of parameters.

These exotic models predict 21-cm signals that, over a significant range of model parameters, are substantially stronger than in any standard astrophysical model. Thus, the exotic models will be some of the earliest models to be constrained by observations, including those by the SKA. Figure 6 shows an estimate of the maximum 21-cm power spectrum for the interacting millicharged dark matter model at wavenumber $k = 0.13$ Mpc $^{-1}$ (right panel, solid blue curve). Interestingly, the maximum power spectrum from this model is comparable to the maximum power spectrum from another major category of models inspired by the EDGES signal, namely, strongly-emitting radio

galaxies (Sec. 5.1). In both cases, the exotic model can yield a 21-cm power spectrum that is 3 orders of magnitude higher than the power spectrum of standard astrophysical models, and 5 orders of magnitude above the expected SKA sensitivity.

5.4 Dark matter annihilation/decay

The fundamental nature of dark matter (DM) has troubled physicists ever since its existence was confirmed since the early 1970s (Rubin and Ford, 1970). Past efforts on both the fronts, theory and observation have shown us that on cosmological scales, DM forms the skeleton of the Universe as seen today, i.e., the large-scale structure of our Universe (Peacock et al., 2001). The currently accepted standard model assumes that DM is cold (CDM) and collisionless, and to a good approximation any non-gravitational interactions of DM are tiny. Yet there are several studies (e.g. Acevedo et al., 2024) which propose DM-ordinary matter interactions to address observational inconsistencies such as the “core-cusp” problem (de Blok, 2010; Oh et al., 2011). We refer the interested readers to Bergström (2009), Bertone and Hooper (2018), and Arbey and Mahmoudi (2021) for a further reading on DM – listing the possible DM candidates, and detection strategies for different types of DM candidates. See Slatyer (2024) to read more about the interacting dark matter scenario from the perspective of cosmology.

Various DM particle models have been proposed, including Weakly Interacting Massive Particles (WIMPs), axions, dark photons, and primordial black holes (PBHs). These candidates are being probed through multiple approaches such as direct detection, collider experiments, and astrophysical observations.

DM particles may annihilate into other Standard Model particles, for example electron-positron pairs, muon pairs, tau lepton pairs, bottom quark pairs, and photon pairs. These annihilation processes inject additional energy into the IGM in the Universe (Slatyer et al., 2009; Slatyer, 2016a,b). Similarly, DM particles may spontaneously decay into lighter Standard Model particles, thereby also releasing energy into the IGM (Chen and Kamionkowski, 2004). These energy injections can heat and ionize the IGM (Liu et al., 2020, 2023; Qin et al., 2024; Sun et al., 2025b), altering its thermal history and inevitably leaving observable cosmological imprints on cosmological 21-cm signal. Conversely, given a dataset it is possible to derive constraints on the fundamental properties of DM (e.g. Mittal et al., 2022).

Current constraints from cosmological and astrophysical probes have placed stringent limits on such energy injection processes. Analysis of CMB polarization anisotropy by the Planck collaboration has set upper limits on the dark matter annihilation efficiency reaching $\sim 3 \times 10^{-28} \text{ cm}^3 \text{ s}^{-1} \text{ GeV}^{-1}$ for the $\chi\chi \rightarrow e^+e^-$ channel and a decay lifetime limit of $\sim 10^{24} \text{ s}$ (Planck Collaboration et al., 2020). Complementary constraints come from Fermi-LAT observations of gamma rays from galaxies and galaxy clusters, yielding an limit on annihilation cross-section $\langle\sigma v\rangle \lesssim 3 \times 10^{-26} \text{ cm}^3 \text{ s}^{-1}$ for $m_\chi = 100 \text{ GeV}$ and on decay lifetime $\tau_\chi \gtrsim 10^{26} \text{ s}$ (Ackermann et al., 2015). Other well-motivated candidates like axions and dark photons also face distinct bounds from CMB and other cosmological probes. For detailed discussions, we refer readers to specialized papers (Bondarenko et al., 2020; Das, 2024; Nguyen et al., 2025). However, probes like the CMB primarily investigate physical processes in the late Universe (from post-reionization to the present day), whereas the 21-cm signal

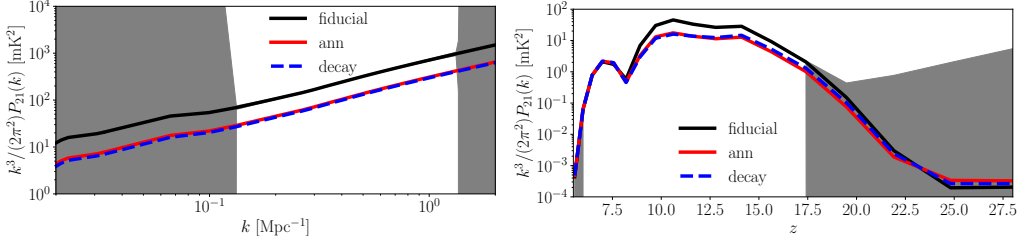


Figure 7: *Left:* The 21 cm power spectra at $z \sim 10$ in the absence (black)/presence of DM annihilation (red) and decay (blue). *Right:* Similar to the left panel, however now the power spectra at $k = 0.05 \text{ Mpc}^{-1}$ as functions of redshift are plotted. In all panels filled regions are SKA-AA* uncertainties for $t_{\text{obs}} = 1080$ hr and bandwidth 10 MHz, calculated by 21cmSense, the left panel adopts moderate foreground removal model, while the right panel assumes optimistic case.

has the potential to open a new window into the DM effects in the earlier Universe stages, i.e., Cosmic Dawn and EoR.

Fig. 7 shows the influence on 21-cm power spectra by annihilation or decay of DM particles with $m_\chi = 100 \text{ GeV}$. For annihilation, $\chi\chi \rightarrow e^+e^-$ channel and $\langle\sigma v\rangle = 3 \times 10^{-26} \text{ cm}^3 \text{ s}^{-1}$ are assumed; for decay, $\chi \rightarrow e^+e^-$ channel and $\tau_\chi = 10^{26} \text{ s}$ are adopted. Compared with the observational uncertainties of SKA-AA*, the effects of DM are distinguishable at least between $k \sim 0.1 - 1 \text{ Mpc}^{-1}$. Moreover, Cosmic Dawn is the optimal stage for detecting DM effects. As before this stage, the IGM has not yet well heated/ionized by DM, therefore the effects are small. After that, the heating and ionization of the IGM is dominated by first galaxies, the DM effects are negligible and are hard to see on the 21-cm signal.

Compared with other cosmological probes, the 21-cm signal is more sensitive to temperature variations in the IGM, enabling the detection of weaker energy injection processes beyond the reach of other probes. Moreover, the 21-cm power spectrum not only provides information about global evolution but also reveals spatial fluctuations, containing richer physical information that helps distinguish DM effects from astrophysical sources. Thus, future 21-cm observations by SKA are expected to provide unique tests of DM nature across different redshift and energy scales, thereby placing stringent constraints on the fundamental nature of DM particles.

5.5 Non-cold dark matter

The first stars and galaxies in the Universe formed when baryons fell into gravitational potential wells created by bound dark matter particles. Consequently, the nature of dark matter significantly influences the properties of these luminous objects, including their typical masses and number densities. In this section, we consider a range of phenomenological dark matter models that affect the gravitational evolution of large-scale structure, such as warm dark matter (WDM; e.g., Sitwell et al., 2014; Giri and Schneider, 2022), fuzzy dark matter (FDM; e.g., Hu et al., 2000; Nebrin et al., 2019; Jones et al., 2021; Giri and Schneider, 2022; Flitter and Kovetz, 2022; Sarkar et al., 2022; Liu et al., 2025b), and the Effective Theory of Structure Formation (ETHOS; e.g., Verwohlt et al., 2024). These models typically characterize dark matter particles by their rest mass energy, with more energetic particles suppressing the formation of small-scale structures. In particular, higher

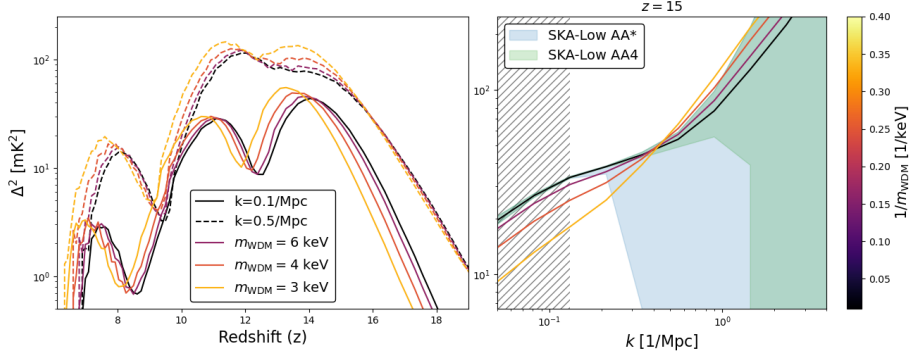


Figure 8: The power spectrum evolution over redshift (left panel) and wavenumber (right panel). The shaded regions correspond to the error due to cosmic variance and instrumental noise ($t_{\text{obs}} = 1000\text{h}$, $\Delta \ln k = 0.5$) with AA* (blue) and AA4 (green) layout of SKA-Low.

particle energies correspond to higher minimum halo masses capable of hosting luminous sources. In this work, we adopt the WDM scenario as a representative case for non-cold dark matter models.

Previous studies have shown that these models are best distinguished at high redshifts during epochs such as cosmic dawn and reionization, where their impact on structure formation is most pronounced (e.g., Dayal and Giri, 2024). Observations of the 21-cm signal by SKA-Low will provide a powerful probe of such models (e.g., Giri and Schneider, 2022). Figure 8 illustrates the evolution of the 21-cm power spectrum for several WDM models, computed using the HMREIO framework (Schneider et al., 2021, 2023). The underlying astrophysical model is fixed to *Model 1* in Schneider et al. (2023), with only the dark matter particle mass (m_{WDM}) being varied. As m_{WDM} decreases, structure formation is progressively delayed, which in turn postpones the heating and reionization of the IGM, as seen in the left panel of Fig. 8. The right panel highlights the potential of SKA-Low to discriminate between these models via 21-cm power spectrum measurements at $z = 15$. The shaded region around the CDM (cold dark matter) curve indicates the combined uncertainties from cosmic variance and instrumental noise. The hatched region marks scales $k \lesssim 0.15 \text{ Mpc}^{-1}$ that are heavily contaminated by foregrounds (Pober et al., 2014; Greig and Mesinger, 2015). Nevertheless, several foreground-free modes remain accessible for ruling out non-cold DM scenarios, even with a 1000-hour observation using the AA* layout. This capability improves substantially with the AA4 configuration, where a greater number of modes become available for discriminating among dark matter models. It is important to note that this sensitivity is redshift-dependent, as the signal-to-noise ratio varies across different epochs.

While our focus here has been on the 21-cm power spectrum, SKA-Low will be powerful enough to enable studies that go well beyond this two-point statistic (e.g., Giri et al., 2018, 2019b; Giri and Mellema, 2021). Several works have demonstrated that complementary observables—such as the 21-cm bispectrum (Saxena et al., 2020), the 21-cm forest (Shimabukuro et al., 2014, 2020b,a; Kawasaki et al., 2021; Shao et al., 2023; Sun et al., 2025), and direct imaging (Neusch et al., 2022; Sabiu et al., 2022)—can further constrain non-cold dark matter models. We refer interested readers to these studies for a broader perspective on how upcoming 21-cm observations may probe the fundamental nature of dark matter.

5.6 Primordial features from inflation

Inflation (Guth, 1981; Linde, 1982; Albrecht and Steinhardt, 1982; Starobinsky, 1980; Sato, 1981; Kazanas, 1980) explains the origin of primordial density perturbations from quantum fluctuations of the early Universe. These fluctuations evolve to form large-scale structures and carry imprints of primordial physics. While current CMB and large-scale structure observations are broadly consistent with a nearly scale-invariant primordial power spectrum, deviations at certain scales may hint at new physics. Several inflationary models predict scale-dependent features in the primordial power spectrum, or “primordial features” (see, e.g., Akrami et al. 2020; Chluba et al. 2015; Beutler et al. 2019 and references therein). The neutral hydrogen distribution at high redshift carries imprints of primordial features through density fluctuation evolution. The 21 cm signal during cosmic dawn directly traces the matter distribution and is ideal for probing primordial features, though extraction is challenging due to parameter degeneracies. The tomographic nature of 21 cm observations helps disentangle such degeneracies (Naik et al., 2023, 2025).

Previous studies have explored various types of primordial features with 21 cm intensity mapping and power spectrum, including oscillatory patterns from resonance or step-like features (Chen et al., 2016; Xu et al., 2016), kink, step and warp shapes (Ballardini et al., 2018), and dips from ultra-slow roll phases (Balaji et al., 2022). As a detailed case study, we focus on bump-like features arising from bursts of particle production during inflation (Chung et al., 2000; Barnaby and Huang, 2009; Pearce et al., 2017), which may occur naturally in models based on higher-dimensional gauge theories (Furuuchi, 2016; Furuuchi et al., 2020). The primordial power spectrum is modeled by the height A_I and location k_{peak} of the bump (Pearce et al., 2017).

Bump-like features enhance correlations in density fluctuations, significantly altering 21 cm brightness temperature fluctuations and power spectra (figure 9). These features also affect the reionization history and global 21 cm profile (Naik et al., 2025; Yoshiura et al., 2018, 2020), primarily through modifications to the halo mass function. As k_{peak} increases, reionization shifts from late- to early-completing scenarios, affecting all observables (Naik et al., 2025). Other types of primordial features are also expected to affect density fluctuations and the halo mass function. Detailed SKA forecasts for these feature types remain to be explored.

In Naik et al. (2023), it was demonstrated that multi-redshift 21-cm power spectra can probe bump-like features within $0.1 \leq k [\text{Mpc}^{-1}] \leq 1.0$ with SKA-Low earlier layout. Figure 9 shows 21 cm power spectra for various bump model parameters (violet) and EoR models (green). The shaded regions indicate 95% uncertainty at different redshifts for the SKA-AA4 layout. Simulations were performed using 21cmFAST (Mesinger et al., 2011; Murray et al., 2020) and the noise estimates were computed with 21cmSense (Murray et al. 2024; Pober et al. 2013, 2014), assuming 6 hours per day of deep field observations for 180 days with optimistic foreground removal. The unique spectral shapes of the models with primordial features show strong k and z dependence. At certain scales and redshifts, primordial feature effects are quite distinct from EoR parameter variations. This demonstrates promising prospects for detecting primordial features with SKA-Low AA4 through combining multi-redshift 21 cm power spectra.

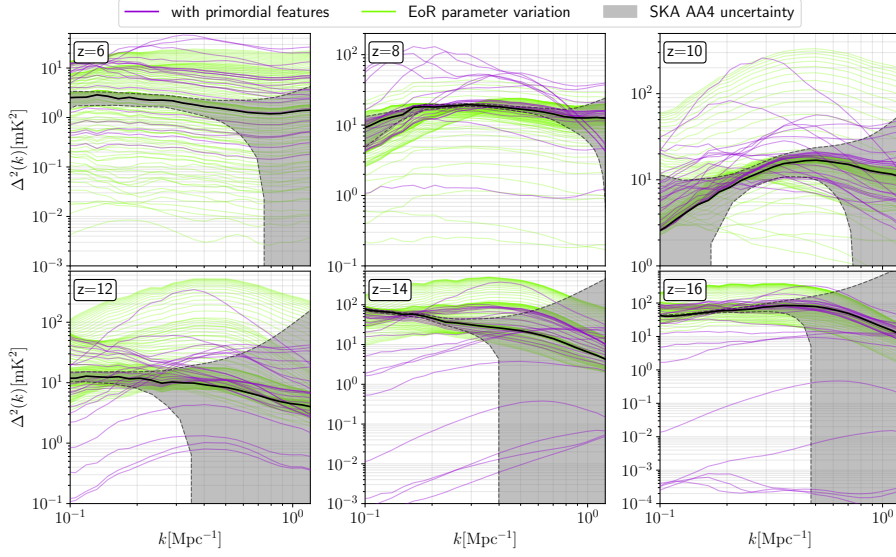


Figure 9: The 21 cm power spectra at different redshifts simulated for the featureless power law model (solid black), models with bump-like features (violet) and various EoR models (green). The shaded region is the 95% uncertainty estimated for SKA-AA4 using 21cmSense.

5.7 Other exotic signatures

Topological defects such as superconducting cosmic strings are predicted by several different extensions to the standard model. If these defects exist, radio emission from their oscillations, cusps and kinks has the potential to modify the 21-cm signal. This is both through direct enhancement of the radio background, and potentially also via soft photon heating (Acharya et al., 2023; Cyr et al., 2024); a poorly-studied yet likely non-negligible effect in models that include a large excess radio background. Current upper limits on the 21-cm power spectrum provide no observational constraints on the existence or properties of cosmic strings (Gessey-Jones et al., 2024), but it has been proposed that SKA 21-cm signal images or three-point statistics could reveal overdensity structures associated with cosmic strings (Hernández, 2014; Maibach et al., 2021).

The inverse Gertsenshtein effect (i.e., conversion of gravitational waves to photons in the presence of a magnetic field) has been posed as a mechanism for detecting high-frequency primordial gravitational waves with radio telescopes (e.g. Domcke and Garcia-Cely, 2021) via the resulting enhancement of the radio background. Forecasts suggest that the SKA may improve current MHz-band constraints on the primordial gravitational wave density parameter Ω_{GW} by 7 – 10 orders of magnitude (He et al., 2024). In principle, all processes that impact halo formation may also leave an imprint in the 21-cm power spectrum, since halo statistics affect galaxy formation, which enables the feedback processes described in Section 2. Some unmentioned examples of such processes include early/dynamical dark energy (Yin, 2023; Adi et al., 2025), free-streaming of massless (Montefalcone et al., 2025) and massive neutrinos (Pritchard and Pierpaoli, 2008; Zhang et al., 2020; Libanore et al., 2025) and isocurvature perturbations (Hotinli et al., 2021; Takeuchi and Chongchitnan, 2014; Qin and Shimabukuro, 2025).

6 Conclusions

In this chapter we have discussed the prospects of the upcoming low-frequency Square Kilometre Array telescope (SKA-Low) to probe standard and exotic signatures from the Cosmic Dawn and the Epoch of Reionization (EoR). The SKA-Low interferometer will be sensitive to frequencies between 50-350 MHz, allowing for a high-precision measurement of the redshifted 21-cm signal from the redshift range of $z \sim 6 - 30$.

The chapter is structured into two main sections discussing standard and exotic signatures from the Cosmic Dawn and the EoR. Among the standard astrophysical signatures, SKA-Low will enable detailed investigations of the first galaxies and their feedback on the IGM. Variations in star-formation efficiency, escape fraction, and duty cycle will modulate the amplitude and scale-dependence of the 21-cm power spectrum, providing constraints on early galaxy formation models beyond the reach of current optical surveys. The imprint of Population III stars, whose intense UV and X-ray radiation initiate the Ly α coupling and early heating, will be reflected in both the timing and morphology of the 21-cm absorption trough. X-ray binaries, expected to dominate the high-energy emission during cosmic dawn, will drive the global transition from absorption to emission, while cosmic rays from early supernovae will produce a spatially extended heating signature detectable through a suppression of small-scale 21-cm power. The presence of supermassive black holes will generate large ionized bubbles and local heating patterns, imprinting scale-dependent anisotropies that SKA-Low can distinguish in its tomographic power-spectrum analysis. Finally, velocity acoustic oscillations (VAOs), arising from baryon-dark-matter streaming velocities, will both modulate star formation in mini-haloes and appear as periodic modulations in the 21-cm power spectrum providing a novel standard ruler for cosmology at high redshifts.

Beyond these standard astrophysical processes, SKA-Low will be sensitive to a wide range of exotic signatures that could reveal new physics beyond the Λ CDM paradigm. These include modifications of the 21-cm signal due to strong radio emitting galaxies or due to the energy injection induced by dark-matter interactions, annihilation or decay, primordial black holes, or primordial magnetic fields. The small-scale clustering could be altered by warm dark matter components, additional hot species, or explicit features imprinted by non-standard inflation. The detection or exclusion of such effects would provide unique constraints on the nature of dark matter, or reveal new and exotic sources.

In summary, the SKA-Low will transform our understanding of the high-redshift Universe and the complex astrophysical processes that shaped it, including the emergence of the very first luminous sources. At the same time, it will serve as a powerful instrument to search for new physics beyond the standard cosmological model, particularly in the dark matter sector. Together, these capabilities will make SKA-Low a cornerstone of early-Universe astrophysics and cosmology.

7 Contributions

A. Schneider coordinated the work on this science chapter and wrote abstract, introduction, and conclusion. S. Mittal led Sec. 2.1 and 5.4, contributed to Sec. 2.2, 4.3, 5.1, and homogenised the bibliography. A. Fialkov led Sec. 2.2 and 4.2, and contributed to sections 4.3 and 5.1. I. T. Iliev

led Sec. 2.3, contributed to Sec. 2.1, 2.2, 4.2 and 4.6. J.Y.H. Chan led Sec. 2.4. S. K. Giri led Sec. 3 and 5.5. R. Barkana led Sec. 4.3, 4.7, and 5.3. A. Bera led Sec. 4.4 and contributed to Sec. 5.2. B. Yue led Sec. 4.5 and Sec. 4.1, and contributed to Sec. 5.4. H. A. G. Cruz and J. Muñoz led Sec. 4.6 and produced Fig. 5. B. Li co-led Sec. 4.7 and contributed to Sec. 5.5. S. Sikder led Sec. 5.1 and made Fig. 5. T. Minoda led Sec. 5.2. S. S. Naik led sec. 5.6 and produced Fig. 9. O. Basquette led Sec. 5.7, contributed to Sec. 4.2 and produced Fig. 3. S. Dasgupta produced Fig. 1. J. Raste contributed to Secs. 2, 2.1, and 2.2. Q. Han and K. Wan contributed to Sec. 2.4. K. K. Datta contributed to Sec. 4.4. M. Zhang contributed to Sec. 4.5. Y. Xu contributed to Sec. 4.5 and Sec. 5.4. M.-L. Zhao contributed to Sec. 5.4. P. Chingangbam contributed to Sec. 5.6.

8 Acknowledgments

RB and SS acknowledge the support of the Israel Science Foundation (grant no. 1078/24). YX acknowledges the support from the National SKA Program of China No. 2020SKA0110401, and the National Key R&D Program of China No. 2022YFF0504300. BY acknowledges the support from the National SKA Program of China No. 2020SKA0110402, and the NSFC International (Regional) Cooperation and Exchange Project No. 12361141814. SM is supported by the ERC (UKRI guaranteed) research grant EP/Y02916X/1.

References

- M. Abdul Karim et al. *Phys. Rev. D*, 112:083515, 2025. doi: 10.1103/tr6y-kpc6.
- J. F. Acevedo et al. *Phys. Rev. D*, 110:083004, 2024. doi: 10.1103/PhysRevD.110.083004.
- S. K. Acharya, B. Cyr, and J. Chluba. *Monthly Notices of the Royal Astronomical Society*, 523 (2):1908–1918, 05 2023. ISSN 0035-8711. doi: 10.1093/mnras/stad1540. URL <https://doi.org/10.1093/mnras/stad1540>.
- M. Ackermann et al. *Phys. Rev. Lett.*, 115(23):231301, Dec. 2015. doi: 10.1103/PhysRevLett.115.231301.
- A. G. Adame et al. *J. Cosmo. Astropart. Phys.*, 2025(2):021, Feb. 2025. doi: 10.1088/1475-7516/2025/02/021.
- T. Adi, J. Flitter, and E. D. Kovetz. *Phys. Rev. D*, 111:043515, Feb 2025. doi: 10.1103/PhysRevD.111.043515. URL <https://link.aps.org/doi/10.1103/PhysRevD.111.043515>.
- K. Ahn. *ApJ*, 830(2):68, Oct. 2016. doi: 10.3847/0004-637X/830/2/68.
- K. Ahn et al. *New Astron. Rev.*, 50(1-3):179–183, Mar. 2006. doi: 10.1016/j.newar.2005.11.021.
- K. Ahn et al. *ApJL*, 756(1):L16, Sept. 2012. doi: 10.1088/2041-8205/756/1/L16.
- Y. Akrami et al. *Astron. Astrophys.*, 641:A10, 2020. doi: 10.1051/0004-6361/201833887.
- S. Alam et al. *MNRAS*, 470(3):2617–2652, Sept. 2017. doi: 10.1093/mnras/stx721.

- A. Albrecht and P. J. Steinhardt. *Phys. Rev. Lett.*, 48:1220–1223, Apr 1982. doi: 10.1103/PhysRevLett.48.1220. URL <https://link.aps.org/doi/10.1103/PhysRevLett.48.1220>.
- C. Alcock and B. Paczynski. *Nature*, 281:358, Oct. 1979. doi: 10.1038/281358a0.
- S. S. Ali, S. Bharadwaj, and B. Pandey. *MNRAS*, 363(1):251–258, Oct. 2005. doi: 10.1111/j.1365-2966.2005.09444.x.
- Y. Ali-Haïmoud, P. D. Meerburg, and S. Yuan. *Phy. Rev. D*, 89(8):083506, Apr. 2014. doi: 10.1103/PhysRevD.89.083506.
- M. A. Alvarez, J. H. Wise, and T. Abel. *ApJL*, 701(2):L133–L137, Aug. 2009. doi: 10.1088/0004-637X/701/2/L133.
- S. Ando and A. Kusenko. *Astrophys. J. Letters*, 722(1):L39–L44, Oct. 2010. doi: 10.1088/2041-8205/722/1/L39.
- P. Anninos, Y. Zhang, T. Abel, and M. L. Norman. *New Astron.*, 2(3):209–224, Aug. 1997. doi: 10.1016/S1384-1076(97)00009-2.
- A. Arbey and F. Mahmoudi. *Prog. Part. Nucl. Phys.*, 119:103865, 2021. doi: <https://doi.org/10.1016/j.pnpnp.2021.103865>.
- D. Babich and A. Loeb. *ApJ*, 635(1):1–10, Dec. 2005. doi: 10.1086/497297.
- S. Baek et al. *A&A*, 495:389, 2009a.
- S. Baek et al. *Astron. Astrophys.*, 495:389, 2009b. doi: 10.1051/0004-6361/200810757.
- S. Baek et al. *A&A*, 523:A4+, Nov. 2010. doi: 10.1051/0004-6361/201014347.
- S. Balaji et al. *Phys. Rev. Lett.*, 129(26):261301, 2022. doi: 10.1103/PhysRevLett.129.261301.
- M. Ballardini, F. Finelli, R. Maartens, and L. Moscardini. *JCAP*, 04:044, 2018. doi: 10.1088/1475-7516/2018/04/044.
- I. Baraffe, A. Heger, and S. E. Woosley. *ApJ*, 550(2):890–896, Apr. 2001. doi: 10.1086/319808.
- L. G. C. Bariuan et al. *MNRAS*, 513(4):4673–4681, July 2022. doi: 10.1093/mnras/stac1153.
- R. Barkana. *MNRAS*, 372(1):259–264, Oct. 2006. doi: 10.1111/j.1365-2966.2006.10882.x.
- R. Barkana. *Nature*, 555(7694):71–74, Mar. 2018a. doi: 10.1038/nature25791.
- R. Barkana. *Nature*, 555(7694):71–74, Mar 2018b. doi: 10.1038/nature25791.
- R. Barkana and A. Loeb. *ApJ*, 609(2):474–481, July 2004. doi: 10.1086/421079.
- R. Barkana and A. Loeb. *ApJL*, 624(2):L65–L68, May 2005a. doi: 10.1086/430599.
- R. Barkana and A. Loeb. *Astrophys. J.*, 626(1):1–11, June 2005b. doi: 10.1086/429954.
- R. Barkana and A. Loeb. *MNRAS*, 372(1):L43–L47, Oct. 2006. doi: 10.1111/j.1745-3933.2006.00222.x.

- R. Barkana, N. J. Outmezguine, D. Redigol, and T. Volansky. *Phy. Rev. D*, 98:103005, Nov. 2018. doi: 10.1103/PhysRevD.98.103005.
- R. Barkana, A. Fialkov, H. Liu, and N. J. Outmezguine. *Phy. Rev. D*, 108(6):063503, Sept. 2023. doi: 10.1103/PhysRevD.108.063503.
- N. Barnaby and Z. Huang. *Phys. Rev. D*, 80:126018, 2009. doi: 10.1103/PhysRevD.80.126018.
- J. E. Bautista et al. *A&A*, 603:A12, June 2017. doi: 10.1051/0004-6361/201730533.
- M. C. Begelman, M. Volonteri, and M. J. Rees. *MNRAS*, 370(1):289–298, July 2006. doi: 10.1111/j.1365-2966.2006.10467.x.
- A. Bera, K. K. Datta, and S. Samui. *MNRAS*, 498(1):918–925, Oct. 2020. doi: 10.1093/mnras/staa1529.
- A. Bera, S. Samui, and K. K. Datta. *MNRAS*, 519(4):4869–4883, 2023. doi: 10.1093/mnras/stac3814.
- L. Bergström. *New J. Phys.*, 11:105006, 2009. doi: 10.1088/1367-2630/11/10/105006.
- A. Berlin, D. Hooper, G. Krnjaic, and S. D. McDermott. *Phys. Rev. Lett.*, 121:011102, Jul 2018. doi: 10.1103/PhysRevLett.121.011102. URL <https://link.aps.org/doi/10.1103/PhysRevLett.121.011102>.
- G. Bertone and D. Hooper. *Rev. Mod. Phys.*, 90:045002, 2018. doi: 10.1103/RevModPhys.90.045002.
- F. Beutler et al. *Phys. Rev. Res.*, 1(3):033209, 2019. doi: 10.1103/PhysRevResearch.1.033209.
- S. Bharadwaj and S. S. Ali. *MNRAS*, 352(1):142–146, July 2004. doi: 10.1111/j.1365-2966.2004.07907.x.
- A. Bhaumik, D. Paul, and S. Pal. *J. Cosmo. Astropart. Phys.*, 2025(1):089, Jan. 2025. doi: 10.1088/1475-7516/2025/01/089.
- M. Bianco et al. *MNRAS*, 504(2):2443–2460, June 2021. doi: 10.1093/mnras/stab787.
- L. Biermann. *Zeitschrift Naturforschung Teil A*, 5:65, Jan. 1950.
- K. Bondarenko, J. Pradler, and A. Sokolenko. *Phys. Lett. B*, 805:135420, 2020. doi: 10.1016/j.physletb.2020.135420.
- S. Bosman. All $z > 5.7$ quasars currently known. Zenodo dataset, Feb. 2020.
- R. J. Bouwens et al. *ApJ*, 811(2):140, Oct. 2015. doi: 10.1088/0004-637X/811/2/140.
- J. Bovy and C. Dvorkin. *ApJ*, 768(1):70, May 2013. doi: 10.1088/0004-637X/768/1/70.
- J. D. Bowman et al. *Nature*, 555:67, 2018. doi: 10.1038/nature25792.
- R. Brandenberger, B. Cyr, and R. Shi. *Journal of Cosmology and Astroparticle Physics*, 2019(9):009, Sept. 2019. doi: 10.1088/1475-7516/2019/09/009.

- A. Brandenburg and K. Subramanian. *Phys. Rep.*, 417(1-4):1–209, Oct. 2005. doi: 10.1016/j.physrep.2005.06.005.
- V. Bromm. *Reports on Progress in Physics*, 76(11):112901, Nov. 2013. doi: 10.1088/0034-4885/76/11/112901.
- V. Bromm and R. B. Larson. *ARA&A*, 42(1):79–118, Sept. 2004. doi: 10.1146/annurev.astro.42.053102.134034.
- S. Buitink et al. *Nature*, 531(7592):70–73, Mar. 2016. doi: 10.1038/nature16976.
- C. Cain et al. *ApJ*, 898(2):168, Aug. 2020. doi: 10.3847/1538-4357/aba26a.
- V. Cammelli et al. *arXiv e-prints*, art. arXiv:2501.17675, Jan. 2025. doi: 10.48550/arXiv.2501.17675.
- J. Cang et al. *Astronomy & Astrophysics*, 698:A152, June 2025. doi: 10.1051/0004-6361/202452982.
- D. Caprioli and A. Spitkovsky. *ApJ*, 783(2):91, Mar. 2014. doi: 10.1088/0004-637X/783/2/91.
- B. J. Carr, J. R. Bond, and W. D. Arnett. *ApJ*, 277:445–469, Feb. 1984. doi: 10.1086/161713.
- D. Ceverino, R. S. Klessen, and S. C. O. Glover. *MNRAS*, 480(4):4842–4850, Nov. 2018. doi: 10.1093/mnras/sty2124.
- J. Y. H. Chan, Q. Han, K. Wu, and J. D. McEwen. *MNRAS*, 531(1):434–449, June 2024. doi: 10.1093/mnras/stae1101.
- X. Chen and J. Miralda-Escudé. *Astrophys. J.*, 602:1, 2004. doi: 10.1086/380829.
- X. Chen, P. D. Meerburg, and M. Münchmeyer. *JCAP*, 09:023, 2016. doi: 10.1088/1475-7516/2016/09/023.
- X.-L. Chen and M. Kamionkowski. *Phys. Rev. D*, 70:043502, 2004. doi: 10.1103/PhysRevD.70.043502.
- M. Chianese, P. Di Bari, K. Farrag, and R. Samanta. *Physics Letters B*, 790:64–70, Mar. 2019. doi: 10.1016/j.physletb.2018.09.040.
- J. Chluba, J. Hamann, and S. P. Patil. *Int. J. Mod. Phys. D*, 24(10):1530023, 2015. doi: 10.1142/S0218271815300232.
- J. Chluba, D. Paoletti, F. Finelli, and J. A. Rubiño-Martín. *MNRAS*, 451(2):2244–2250, Aug. 2015. doi: 10.1093/mnras/stv1096.
- T. R. Choudhury and A. Chakraborty. *arXiv e-prints*, art. arXiv:2504.03384, Apr. 2025. doi: 10.48550/arXiv.2504.03384.
- N. Choustikov et al. *MNRAS*, 537(3):2273–2290, Mar. 2025. doi: 10.1093/mnras/staf126.
- D. J. H. Chung, E. W. Kolb, A. Riotto, and I. I. Tkachev. *Phys. Rev.*, D62:043508, 2000. doi: 10.1103/PhysRevD.62.043508.

- L. Chuzhoy and P. R. Shapiro. *Astrophys. J.*, 651:1, 2006. doi: 10.1086/507670.
- L. Chuzhoy and P. R. Shapiro. *ApJ*, 655:843–846, 2007. doi: 10.1086/510146.
- B. Ciardi, R. Salvaterra, and T. Di Matteo. *MNRAS*, 401(4):2635–2640, Feb. 2010. doi: 10.1111/j.1365-2966.2009.15843.x.
- L. Conaboy et al. *MNRAS*, 525(4):5479–5491, Nov. 2023. doi: 10.1093/mnras/stad2699.
- J. J. Condon et al. *Astrophysical Journal*, 758(1):23, Oct. 2012. doi: 10.1088/0004-637X/758/1/23.
- A. Cooray and S. R. Furlanetto. *MNRAS*, 359(1):L47–L52, May 2005. doi: 10.1111/j.1745-3933.2005.00035.x.
- H. A. G. Cruz et al. *Phy. Rev. D*, 109(2):023518, Jan. 2024. doi: 10.1103/PhysRevD.109.023518.
- H. A. G. Cruz, J. B. Muñoz, N. Sabti, and M. Kamionkowski. *Phy. Rev. D*, 111(8):083503, Apr. 2025. doi: 10.1103/PhysRevD.111.083503.
- B. Cyr, S. K. Acharya, and J. Chluba. *Monthly Notices of the Royal Astronomical Society*, 534(1): 738–757, 09 2024. ISSN 0035-8711. doi: 10.1093/mnras/stae2113. URL <https://doi.org/10.1093/mnras/stae2113>.
- N. Dalal, U.-L. Pen, and U. Seljak. *J. Cosmo. Astropart. Phys.*, 2010(11):007, Nov. 2010. doi: 10.1088/1475-7516/2010/11/007.
- C. R. Das. In *7th International Conference on Particle Physics and Astrophysics*, 12 2024.
- K. K. Datta et al. *MNRAS*, 424(3):1877–1891, Aug. 2012. doi: 10.1111/j.1365-2966.2012.21293.x.
- K. K. Datta et al. *MNRAS*, 442(2):1491–1506, Aug. 2014. doi: 10.1093/mnras/stu927.
- K. K. Datta, A. Kundu, A. Paul, and A. Bera. *Phy. Rev. D*, 102(8):083502, Oct. 2020. doi: 10.1103/PhysRevD.102.083502.
- P. Dayal and S. K. Giri. *Monthly Notices of the Royal Astronomical Society*, 528(2):2784–2789, 2024.
- S. De and H. Tashiro. *Phy. Rev. D*, 89(12):123002, June 2014. doi: 10.1103/PhysRevD.89.123002.
- W. J. G. de Blok. *Advances in Astronomy*, 2010:789293, 2010. doi: <https://doi.org/10.1155/2010/789293>.
- DESI Collaboration et al. *arXiv e-prints*, art. arXiv:1611.00036, Oct. 2016. doi: 10.48550/arXiv.1611.00036.
- V. Domcke and C. Garcia-Cely. *Physical review letters*, 126(2):021104, 2021.
- J. Dowell and G. B. Taylor. *Astrophys. J.*, 858:L9, 2018. doi: 10.3847/2041-8213/aabf86.
- R. Durrer and A. Neronov. *Astron. Astrophys. Rev.*, 21:62, June 2013. doi: 10.1007/s00159-013-0062-7.

- C. Dvorkin, K. Blum, and M. Kamionkowski. *Phy. Rev. D*, 89(2):023519, Jan. 2014. doi: 10.1103/PhysRevD.89.023519.
- M. B. Eide et al. *MNRAS*, 476(1):1174–1190, May 2018. doi: 10.1093/mnras/sty272.
- D. J. Eisenstein and W. Hu. *ApJ*, 496(2):605–614, Mar. 1998. doi: 10.1086/305424.
- J. Fan, H. Chen, C. Avestruz, and A. Khadir. *ApJ*, 979(2):150, Feb. 2025. doi: 10.3847/1538-4357/adald3.
- C. Feng and G. Holder. *ApJL*, 858(2):L17, May 2018. doi: 10.3847/2041-8213/aac0fe.
- A. Fialkov and R. Barkana. *MNRAS*, 445(1):213–224, Nov. 2014. doi: 10.1093/mnras/stu1744.
- A. Fialkov and R. Barkana. *MNRAS*, 486(2):1763–1773, June 2019. doi: 10.1093/mnras/stz873.
- A. Fialkov, R. Barkana, D. Tseliakhovich, and C. M. Hirata. *MNRAS*, 424(2):1335–1345, Aug. 2012. doi: 10.1111/j.1365-2966.2012.21318.x.
- A. Fialkov et al. *MNRAS*, 432(4):2909–2916, July 2013. doi: 10.1093/mnras/stt650.
- A. Fialkov, R. Barkana, and E. Visbal. *Nature*, 506:197–199, 2014. doi: 10.1038/nature12999.
- A. Fialkov, R. Barkana, and A. Cohen. *Phy. Rev. Lett.*, 114(10):101303, Mar. 2015. doi: 10.1103/PhysRevLett.114.101303.
- A. Fialkov, A. Cohen, R. Barkana, and J. Silk. *MNRAS*, 464(3):3498–3508, 2017. doi: 10.1093/mnras/stw2540.
- G. B. Field. *Proceedings of the IRE*, 46:240–250, Jan. 1958. doi: 10.1109/JRPROC.1958.286741.
- D. J. Fixsen et al. *Astrophys. J.*, 734:5, 2011. doi: 10.1088/0004-637x/734/1/5.
- J. Flitter and E. D. Kovetz. *Physical Review D*, 106(6):063504, 2022.
- E. B. Fomalont et al. *Astronomical Journal*, 96:1187, Oct. 1988. doi: 10.1086/114872.
- T. Fragos et al. *ApJ*, 764(1):41, Feb. 2013a. doi: 10.1088/0004-637X/764/1/41.
- T. Fragos et al. *ApJL*, 776(2):L31, Oct. 2013b. doi: 10.1088/2041-8205/776/2/L31.
- S. Fraser et al. *Physics Letters B*, 785:159–164, Oct. 2018. doi: 10.1016/j.physletb.2018.08.035.
- W. L. Freedman et al. *ApJ*, 985(2):203, June 2025. doi: 10.3847/1538-4357/adce78.
- S. R. Furlanetto. *MNRAS*, 371:867–878, 08 2006. doi: 10.1111/j.1365-2966.2006.10725.x.
- S. R. Furlanetto and A. Loeb. *ApJ*, 611:642, 2004. doi: 10.1086/422242.
- S. R. Furlanetto and J. R. Pritchard. *MNRAS*, 372:1093, 2006. doi: 10.1111/j.1365-2966.2006.10899.x.
- S. R. Furlanetto, M. Zaldarriaga, and L. Hernquist. *The Astrophysical Journal*, 613(1):1, 2004.
- K. Furuuchi. *JCAP*, 1607(07):008, 2016. doi: 10.1088/1475-7516/2016/07/008.

- K. Furuuchi, S. S. Naik, and N. J. Jobu. *JCAP*, 06:054, 2020. doi: 10.1088/1475-7516/2020/06/054.
- I. Georgiev, G. Mellema, and S. K. Giri. *MNRAS*, 536(4):3689–3706, Feb. 2025. doi: 10.1093/mnras/stae2788.
- T. Gessey-Jones et al. *MNRAS*, 516(1):841–860, Oct. 2022. doi: 10.1093/mnras/stac2049.
- T. Gessey-Jones et al. *MNRAS*, 526(3):4262–4284, Dec. 2023. doi: 10.1093/mnras/stad3014.
- T. Gessey-Jones et al. *Monthly Notices of the Royal Astronomical Society*, 529(1):519–536, 2024.
- T. Gessey-Jones et al. *Nature Astronomy*, June 2025. doi: 10.1038/s41550-025-02575-x.
- R. Ghara et al. *MNRAS*, 476(2):1741–1755, May 2018. doi: 10.1093/mnras/sty314.
- R. Ghara et al. *Monthly Notices of the Royal Astronomical Society*, 493(4):4728–4747, 2020.
- V. L. Ginzburg and L. M. Ozernoi. *Sov. Astron.*, 9:726, Apr. 1966.
- S. Giri, G. Mellema, and H. Jensen. *Journal of Open Source Software*, 5(52):2363, 2020.
- S. K. Giri and G. Mellema. *Monthly Notices of the Royal Astronomical Society*, 505(2):1863–1877, 2021.
- S. K. Giri and A. Schneider. *Physical review D*, 105(8):083011, 2022.
- S. K. Giri, G. Mellema, and R. Ghara. *Monthly Notices of the Royal Astronomical Society*, 479(4):5596–5611, 2018.
- S. K. Giri et al. *Journal of Cosmology and Astroparticle Physics*, 2019(02):058, 2019a.
- S. K. Giri et al. *Monthly Notices of the Royal Astronomical Society*, 489(2):1590–1605, 2019b.
- S. K. Giri et al. *MNRAS*, 533(2):2364–2378, Sept. 2024. doi: 10.1093/mnras/stae1999.
- F. Govoni and L. Feretti. *International Journal of Modern Physics D*, 13(8):1549–1594, Jan. 2004. doi: 10.1142/S0218271804005080.
- T. H. Greif, S. D. M. White, R. S. Klessen, and V. Springel. *ApJ*, 736(2):147, Aug. 2011. doi: 10.1088/0004-637X/736/2/147.
- B. Greig and A. Mesinger. *Mon. Not. Roy. Astron. Soc.*, 449(4):4246–4263, 2015. doi: 10.1093/mnras/stv571.
- H. J. Grimm, M. Gilfanov, and R. Sunyaev. *MNRAS*, 339(3):793–809, Mar. 2003. doi: 10.1046/j.1365-8711.2003.06224.x.
- G. Gürkan et al. *MNRAS*, 475(3):3010–3028, Apr. 2018. doi: 10.1093/mnras/sty016.
- A. H. Guth. *Phys. Rev. D*, 23:347–356, Jan 1981. doi: 10.1103/PhysRevD.23.347. URL <https://link.aps.org/doi/10.1103/PhysRevD.23.347>.
- Z. Haiman, M. J. Rees, and A. Loeb. *ApJ*, 467:522, Aug. 1996. doi: 10.1086/177628.
- Y. Harikane et al. *ApJ*, 959(1):39, Dec. 2023. doi: 10.3847/1538-4357/ad029e.

- M. J. Hayes et al. *ApJL*, 971(1):L16, Aug. 2024. doi: 10.3847/2041-8213/ad63a7.
- Y. He et al. *Journal of Cosmology and Astroparticle Physics*, 2024(05):051, 2024.
- G. Heald et al. *Galaxies*, 8(3):53, July 2020. doi: 10.3390/galaxies8030053.
- S. Hegde and S. R. Furlanetto. *MNRAS*, 525(1):428–447, Oct. 2023. doi: 10.1093/mnras/stad2308.
- S. Hegde and S. R. Furlanetto. *The Open Journal of Astrophysics*, 8:147, Oct. 2025. doi: 10.33232/001c.145070.
- A. Heger and S. E. Woosley. *ApJ*, 567(1):532–543, Mar. 2002. doi: 10.1086/338487.
- HERA Collaboration et al. *ApJ*, 945(2):124, Mar. 2023. doi: 10.3847/1538-4357/acaf50.
- O. F. Hernández. *Phys. Rev. D*, 90:123504, Dec 2014. doi: 10.1103/PhysRevD.90.123504. URL <https://link.aps.org/doi/10.1103/PhysRevD.90.123504>.
- A. M. Hillas. *Journal of Physics G Nuclear Physics*, 31(5):R95–R131, May 2005. doi: 10.1088/0954-3899/31/5/R02.
- S. Hirano, N. Yoshida, Y. Sakurai, and M. S. Fujii. *ApJ*, 855(1):17, Mar. 2018. doi: 10.3847/1538-4357/aaaaba.
- C. M. Hirata, A. Mishra, and T. Venumadhav. *Phys. Rev. D*, 97(10):103521, May 2018. doi: 10.1103/PhysRevD.97.103521.
- P. Hirling et al. *Astronomy and Computing*, 48:100861, July 2024. doi: 10.1016/j.ascom.2024.100861.
- G. P. Holder. *ApJ*, 780(1):112, Jan. 2014. doi: 10.1088/0004-637X/780/1/112.
- L. N. Holzbauer and S. R. Furlanetto. *MNRAS*, 419(1):718–731, Jan. 2012. doi: 10.1111/j.1365-2966.2011.19752.x.
- S. C. Hotinli et al. *Phys. Rev. D*, 104(6):063536, Sept. 2021. doi: 10.1103/PhysRevD.104.063536.
- S. C. Hotinli, D. J. E. Marsh, and M. Kamionkowski. *Phys. Rev. D*, 106(4):043529, Aug. 2022. doi: 10.1103/PhysRevD.106.043529.
- W. Hu, R. Barkana, and A. Gruzinov. *Phys. Rev. Lett.*, 85(6):1158–1161, Aug. 2000. doi: 10.1103/PhysRevLett.85.1158.
- T. Huege et al. In *European Physical Journal Web of Conferences*, volume 135 of *European Physical Journal Web of Conferences*, page 02003. EDP, Mar. 2017. doi: 10.1051/epjconf/201713502003.
- I. T. Iliev et al. *MNRAS*, 369(4):1625–1638, July 2006. doi: 10.1111/j.1365-2966.2006.10502.x.
- I. T. Iliev et al. *MNRAS*, 423(3):2222–2253, July 2012. doi: 10.1111/j.1365-2966.2012.21032.x.
- J. Jaacks, K. Nagamine, and J. H. Choi. *MNRAS*, 427(1):403–414, Nov. 2012. doi: 10.1111/j.1365-2966.2012.21989.x.
- R. Jana and B. B. Nath. *MNRAS*, 479(1):153–161, Sept. 2018. doi: 10.1093/mnras/sty1481.

- R. Jana, B. B. Nath, and P. L. Biermann. *MNRAS*, 483(4):5329–5333, Mar. 2019. doi: 10.1093/mnras/sty3426.
- H. Jensen et al. *MNRAS*, 435(1):460–474, Oct. 2013. doi: 10.1093/mnras/stt1341.
- L. Ji, M. Kamionkowski, and K. Inomata. *Phy. Rev. D*, 103(2):023516, Jan. 2021. doi: 10.1103/PhysRevD.103.023516.
- L. Ji, S. C. Hotinli, and M. Kamionkowski. *Phy. Rev. D*, 107(12):123533, June 2023. doi: 10.1103/PhysRevD.107.123533.
- M. Johnston-Hollitt et al. In *Advancing Astrophysics with the Square Kilometre Array (AASKA14)*, page 92, Apr. 2015. doi: 10.22323/1.215.0092.
- D. Jones et al. *The Astrophysical Journal*, 913(1):7, 2021.
- N. Kaiser. *MNRAS*, 227:1–21, July 1987. doi: 10.1093/mnras/227.1.1.
- H. Kang and P. R. Shapiro. *ApJ*, 386:432, Feb. 1992. doi: 10.1086/171029.
- O. Z. Katz, D. Redigolo, and T. Volansky. *J. Cosmo. Astropart. Phys.*, 2025(10):047, Oct. 2025. doi: 10.1088/1475-7516/2025/10/047.
- M. Kawasaki, W. Nakano, H. Nakatsuka, and E. Sonomoto. *Journal of Cosmology and Astroparticle Physics*, 2021(04):019, 2021.
- D. Kazanas. *ApJL*, 241:L59–L63, Oct. 1980. doi: 10.1086/183361.
- J. Kennedy et al. *MNRAS*, 529(4):3684–3698, Apr. 2024. doi: 10.1093/mnras/stae760.
- E.-J. Kim, A. V. Olinto, and R. Rosner. *Astrophys. J.*, 468:28, Sept. 1996. doi: 10.1086/177667.
- R. S. Klessen and S. C. O. Glover. *ARA&A*, 61:65–130, Aug. 2023. doi: 10.1146/annurev-astro-071221-053453.
- E. D. Kovetz et al. *Phy. Rev. D*, 98(10):103529, Nov. 2018. doi: 10.1103/PhysRevD.98.103529.
- M. Kuhlen, P. Madau, and R. Montgomery. *ApJL*, 637(1):L1–L4, Jan. 2006. doi: 10.1086/500548.
- K. E. Kunze. *J. Cosmo. Astropart. Phys.*, 2019(1):033, Jan. 2019. doi: 10.1088/1475-7516/2019/01/033.
- P. La Plante et al. *ApJ*, 789(1):31, July 2014. doi: 10.1088/0004-637X/789/1/31.
- R. B. Larson and S. Starrfield. *A&A*, 13:190, July 1971.
- A. J. Lee et al. *ApJ*, 985(2):182, June 2025. doi: 10.3847/1538-4357/adc8a1.
- B. D. Lehmer et al. *ApJ*, 724(1):559–571, Nov. 2010. doi: 10.1088/0004-637X/724/1/559.
- B. D. Lehmer et al. *ApJ*, 825(1):7, July 2016. doi: 10.3847/0004-637X/825/1/7.
- B. D. Lehmer et al. *ApJ*, 907(1):17, Jan. 2021. doi: 10.3847/1538-4357/abcec1.
- N. Leite et al. *MNRAS*, 469(1):416–424, July 2017. doi: 10.1093/mnras/stx805.

- J. S. W. Lewis et al. *MNRAS*, 516(3):3389–3397, Nov. 2022. doi: 10.1093/mnras/stac2383.
- B. Li, J. Tan, and Y. Mao. *ApJ*, 918(1):14, Sept. 2021. doi: 10.3847/1538-4357/ac09e4.
- S. Libanore et al. *Phys. Rev. D*, 112(6):063502, Sept. 2025. doi: 10.1103/tdms-6n76.
- A. Linde. *Physics Letters B*, 108(6):389–393, 1982. ISSN 0370-2693. doi: [https://doi.org/10.1016/0370-2693\(82\)91219-9](https://doi.org/10.1016/0370-2693(82)91219-9). URL <https://www.sciencedirect.com/science/article/pii/S0370269382912199>.
- B. Liu et al. *MNRAS*, 541(4):3113–3133, Aug. 2025a. doi: 10.1093/mnras/staf1178.
- H. Liu, N. J. Outmezguine, D. Redigolo, and T. Volansky. *Phys. Rev. D*, 100:123011, Dec 2019. doi: 10.1103/PhysRevD.100.123011. URL <https://link.aps.org/doi/10.1103/PhysRevD.100.123011>.
- H. Liu, G. W. Ridgway, and T. R. Slatyer. *Phys. Rev. D*, 101:023530, 2020. doi: 10.1103/PhysRevD.101.023530.
- H. Liu, W. Qin, G. W. Ridgway, and T. R. Slatyer. *Phys. Rev. D*, 108(4):043530, 2023. doi: 10.1103/PhysRevD.108.043530.
- S. Liu et al. *Phys. Rev. D*, 112(10):103534, Nov. 2025b. doi: 10.1103/zh2b-hhrs.
- A. Loeb and G. B. Rybicki. *Astrophys. J.*, 524:527, 1999. doi: 10.1086/307844.
- T. Louis et al. *arXiv e-prints*, art. arXiv:2503.14452, Mar. 2025. doi: 10.48550/arXiv.2503.14452.
- Q. Ma, B. Ciardi, M. B. Eide, and K. Helgason. *MNRAS*, 480(1):26–34, Oct. 2018. doi: 10.1093/mnras/sty1806.
- Q.-B. Ma et al. *MNRAS*, 522(3):3284–3297, July 2023. doi: 10.1093/mnras/stad1203.
- P. Madau, A. Meiksin, and M. J. Rees. *ApJ*, 475:429–444, 1997. doi: 10.1086/303549.
- P. Madau et al. *Astrophys. J.*, 604(2):484–494, apr 2004. doi: 10.1086/381935.
- D. Maibach, R. Brandenberger, D. Crichton, and A. Refregier. *Phys. Rev. D*, 104:123535, Dec 2021. doi: 10.1103/PhysRevD.104.123535. URL <https://link.aps.org/doi/10.1103/PhysRevD.104.123535>.
- R. Maiolino et al. *Nature*, 627(8002):59–63, Mar. 2024. doi: 10.1038/s41586-024-07052-5.
- Y. Mao et al. *MNRAS*, 422(2):926–954, May 2012. doi: 10.1111/j.1365-2966.2012.20471.x.
- J. Matthee et al. *ApJ*, 963(2):129, Mar. 2024. doi: 10.3847/1538-4357/ad2345.
- M. McQuinn et al. *ApJ*, 653(2):815–834, Dec. 2006. doi: 10.1086/505167.
- R. H. Mebane, J. Mirocha, and S. R. Furlanetto. *MNRAS*, 493(1):1217–1226, Mar. 2020. doi: 10.1093/mnras/staa280.
- A. Meiksin. *Research Notes of the American Astronomical Society*, 5(5):126, May 2021. doi: 10.3847/2515-5172/ac053d.

- G. Mellema, I. T. Iliev, M. Alvarez, and P. R. Shapiro. *NewA*, 11:374, 2006.
- G. Mellema et al. *Experimental Astronomy*, 36(1):235–318, 2013.
- A. Mesinger, S. Furlanetto, and R. Cen. *MNRAS*, 411:955–972, 2011. doi: 10.1111/j.1365-2966.2010.17731.x.
- S. Mineo, M. Gilfanov, and R. Sunyaev. *MNRAS*, 419(3):2095–2115, Jan. 2012. doi: 10.1111/j.1365-2966.2011.19862.x.
- S. Mineo et al. *MNRAS*, 437(2):1698–1707, Jan. 2014. doi: 10.1093/mnras/stt1999.
- T. Minoda, H. Tashiro, and T. Takahashi. *MNRAS*, 488(2):2001–2005, Sept. 2019. doi: 10.1093/mnras/stz1860.
- I. F. Mirabel et al. *A&A*, 528:A149, Apr. 2011. doi: 10.1051/0004-6361/201016357.
- J. Mirocha and S. R. Furlanetto. *MNRAS*, 483(2):1980–1992, Feb. 2019. doi: 10.1093/mnras/sty3260.
- J. Mirocha et al. *MNRAS*, 478(4):5591–5606, Aug. 2018. doi: 10.1093/mnras/sty1388.
- A. Mishra and C. M. Hirata. *Phy. Rev. D*, 97(10):103522, May 2018. doi: 10.1103/PhysRevD.97.103522.
- S. Mittal and G. Kulkarni. *MNRAS*, 503:4264, 2020. doi: 10.1093/mnras/staa3811.
- S. Mittal and G. Kulkarni. *MNRAS*, 510:4992, 2022a. doi: 10.1093/mnras/stac005.
- S. Mittal and G. Kulkarni. *MNRAS*, 515:2901, 2022b. doi: 10.1093/mnras/stac1961.
- S. Mittal, A. Ray, G. Kulkarni, and B. Dasgupta. *J. Cosmo. Astropart. Phys.*, 2022:030, 2022. doi: 10.1088/1475-7516/2022/03/030.
- S. Mittal, G. Kulkarni, and T. Garel. *MNRAS*, 535:1979, 2024. doi: 10.1093/mnras/stae2468.
- S. Mittal, G. Kulkarni, and P. Sims. *RAS Tech. Instrum.*, 5:rzag001, 2026. doi: 10.1093/rasti/rzag001.
- R. Mondal et al. *MNRAS*, 483(1):L109–L113, Feb. 2019. doi: 10.1093/mnrasl/sly226.
- R. Mondal et al. *MNRAS*, 494(3):4043–4056, 04 2020. ISSN 0035-8711. doi: 10.1093/mnras/staa1026. URL <https://doi.org/10.1093/mnras/staa1026>.
- G. Montefalcone et al. *arXiv e-prints*, art. arXiv:2509.03595, Sept. 2025. doi: 10.48550/arXiv.2509.03595.
- J. B. Muñoz. *Phy. Rev. Lett.*, 123(13):131301, Sept. 2019. doi: 10.1103/PhysRevLett.123.131301.
- J. B. Muñoz and F.-Y. Cyr-Racine. *Phy. Rev. D*, 103(2):023512, Jan. 2021. doi: 10.1103/PhysRevD.103.023512.
- J. B. Muñoz and A. Loeb. *J. Cosmo. Astropart. Phys.*, 2017(11):043, Nov. 2017. doi: 10.1088/1475-7516/2017/11/043.

- J. B. Muñoz and A. Loeb. *Nature*, 557(7707):684–686, May 2018. doi: 10.1038/s41586-018-0151-x.
- J. B. Muñoz, E. D. Kovetz, and Y. Ali-Haïmoud. *Phy. Rev. D*, 92(8):083528, Oct. 2015. doi: 10.1103/PhysRevD.92.083528.
- J. B. Muñoz, C. Dvorkin, and A. Loeb. *Phy. Rev. Lett.*, 121(12):121301, Sept. 2018. doi: 10.1103/PhysRevLett.121.121301.
- J. B. Muñoz et al. *MNRAS*, 511(3):3657–3681, Apr. 2022. doi: 10.1093/mnras/stac185.
- J. B. Muñoz. *Monthly Notices of the Royal Astronomical Society*, 523(2):2587–2607, 2023.
- J. B. Muñoz, C. Dvorkin, and F.-Y. Cyr-Racine. *Phys. Rev. D*, 101(6):063526, 2020. doi: 10.1103/PhysRevD.101.063526.
- S. Murray, J. Pober, and M. Kolopanis. *The Journal of Open Source Software*, 9(97):6501, 2024.
- S. G. Murray et al. *J. Open Source Softw.*, 5(54):2582, 2020. doi: 10.21105/joss.02582.
- S. S. Naik, P. Chingangbam, and K. Furuuchi. *JCAP*, 04:058, 2023. doi: 10.1088/1475-7516/2023/04/058.
- S. S. Naik et al. *JCAP*, 05:038, 2025. doi: 10.1088/1475-7516/2025/05/038.
- S. Naoz, N. Yoshida, and N. Y. Gnedin. *ApJ*, 747(2):128, Mar. 2012. doi: 10.1088/0004-637X/747/2/128.
- S. Naoz, N. Yoshida, and N. Y. Gnedin. *ApJ*, 763(1):27, Jan. 2013. doi: 10.1088/0004-637X/763/1/27.
- P. Natarajan et al. *ApJL*, 960(1):L1, Jan. 2024. doi: 10.3847/2041-8213/ad0e76.
- B. B. Nath and P. L. Biermann. *MNRAS*, 265:241–249, Nov. 1993. doi: 10.1093/mnras/265.1.241.
- O. Nebrin, R. Ghara, and G. Mellema. *Journal of Cosmology and Astroparticle Physics*, 2019(04):051, 2019.
- A. Neronov and I. Vovk. *Science*, 328(5974):73, Apr. 2010. doi: 10.1126/science.1184192.
- S. Neutsch, C. Heneka, and M. Brüggén. *Monthly Notices of the Royal Astronomical Society*, 511(3):3446–3462, 2022.
- T. T. Q. Nguyen et al. *arXiv e-prints*, 7 2025.
- L. Noble et al. *J. Cosmo. Astropart. Phys.*, 2024(10):003, Oct. 2024. doi: 10.1088/1475-7516/2024/10/003.
- A. Nusser. *MNRAS*, 364(2):743–750, Dec. 2005. doi: 10.1111/j.1365-2966.2005.09603.x.
- P. Ocvirk et al. *MNRAS*, 496(4):4087–4107, Aug. 2020. doi: 10.1093/mnras/staa1266.
- S.-H. Oh et al. *Astron. J.*, 141:193, 2011. doi: 10.1088/0004-6256/141/6/193.
- S. P. Oh. *ApJ*, 553(2):499–512, June 2001. doi: 10.1086/320957.

- R. M. O’Leary and M. McQuinn. *ApJ*, 760(1):4, Nov. 2012. doi: 10.1088/0004-637X/760/1/4.
- B. W. O’Shea, J. H. Wise, H. Xu, and M. L. Norman. *ApJL*, 807(1):L12, July 2015. doi: 10.1088/2041-8205/807/1/L12.
- F. Pacucci and A. Ferrara. *MNRAS*, 448(1):104–118, Mar. 2015. doi: 10.1093/mnras/stv018.
- F. Pacucci, A. Mesinger, S. Mineo, and A. Ferrara. *MNRAS*, 443(1):678–686, Sept. 2014. doi: 10.1093/mnras/stu1240.
- A. Pallottini et al. *MNRAS*, 440(3):2498–2518, May 2014. doi: 10.1093/mnras/stu451.
- H. Park et al. *ApJ*, 908(1):96, Feb. 2021. doi: 10.3847/1538-4357/abd7f4.
- H. Park et al. *Nature Astronomy*, Sept. 2025. doi: 10.1038/s41550-025-02637-0.
- J. Park, A. Mesinger, B. Greig, and N. Gillet. *MNRAS*, 484(1):933–949, Mar. 2019. doi: 10.1093/mnras/stz032.
- J. A. Peacock et al. *Nature*, 410:169, 2001. doi: 10.1038/35065528.
- L. Pearce, M. Peloso, and L. Sorbo. *JCAP*, 1705(05):054, 2017. doi: 10.1088/1475-7516/2017/05/054.
- Planck Collaboration et al. *A&A*, 641:A6, Sept. 2020. doi: 10.1051/0004-6361/201833910.
- J. C. Pober et al. *AJ*, 145(3):65, Mar. 2013. doi: 10.1088/0004-6256/145/3/65.
- J. C. Pober et al. *ApJ*, 782(2):66, Feb. 2014. doi: 10.1088/0004-637X/782/2/66.
- J. C. Pober et al. *The Astrophysical Journal*, 782(2):66, 2014.
- S. Pochinda et al. *MNRAS*, 531(1):1113–1132, June 2024. doi: 10.1093/mnras/stae1185.
- M. Pospelov, J. Pradler, J. T. Ruderman, and A. Urbano. *Phys. Rev. Lett.*, 121(3):031103, July 2018. doi: 10.1103/PhysRevLett.121.031103.
- A. Pouquet, U. Frisch, and J. Leorat. *Journal of Fluid Mechanics*, 77:321–354, Sept. 1976. doi: 10.1017/S0022112076002140.
- C. Power, G. James, C. Combet, and G. Wynn. *ApJ*, 764:76, 2013. doi: 10.1088/0004-637x/764/1/76.
- J. R. Pritchard and S. R. Furlanetto. *MNRAS*, 376(4):1680–1694, 2007. doi: 10.1111/j.1365-2966.2007.11519.x.
- J. R. Pritchard and E. Pierpaoli. *Phys. Rev. D*, 78:065009, Sep 2008. doi: 10.1103/PhysRevD.78.065009. URL <https://link.aps.org/doi/10.1103/PhysRevD.78.065009>.
- W. Qin, J. B. Muñoz, H. Liu, and T. R. Slatyer. *Phy. Rev. D*, 109(10):103026, May 2024. doi: 10.1103/PhysRevD.109.103026.
- Y. Qin et al. *MNRAS*, 495(1):123–140, June 2020. doi: 10.1093/mnras/staa1131.

- Y. Qin, A. Mesinger, B. Greig, and J. Park. *MNRAS*, 501(4):4748–4758, Mar. 2021. doi: 10.1093/mnras/staa3408.
- Z. Qin and H. Shimabukuro, 2025. URL <https://arxiv.org/abs/2509.14751>.
- A. Rahimieh, P. Parashari, and V. Gluscevic. *MNRAS*, 542(2):1605–1615, Sept. 2025. doi: 10.1093/mnras/staf1326.
- J. Raste, A. K. Sarkar, and S. K. Sethi. *Astrophys. J.*, 976:236, 2024. doi: 10.3847/1538-4357/ad84ec.
- I. Reis, A. Fialkov, and R. Barkana. *MNRAS*, 499(4):5993–6008, Dec. 2020. doi: 10.1093/mnras/staa3091.
- I. Reis, A. Fialkov, and R. Barkana. *MNRAS*, 506:5479, 2021. doi: 10.1093/mnras/stab2089.
- M. Ricotti and J. P. Ostriker. *MNRAS*, 352(2):547–562, Aug. 2004. doi: 10.1111/j.1365-2966.2004.07942.x.
- A. G. Riess et al. *ApJ*, 876(1):85, May 2019. doi: 10.3847/1538-4357/ab1422.
- A. G. Riess et al. *ApJL*, 934(1):L7, July 2022. doi: 10.3847/2041-8213/ac5c5b.
- A. G. Riess et al. *ApJ*, 977(1):120, Dec. 2024. doi: 10.3847/1538-4357/ad8c21.
- H. E. Ross, K. L. Dixon, I. T. Iliev, and G. Mellema. *MNRAS*, 468(4):3785–3797, July 2017. doi: 10.1093/mnras/stx649.
- H. E. Ross et al. *Monthly Notices of the Royal Astronomical Society*, 506(3):3717–3733, 2021.
- V. C. Rubin and J. Ford, W. Kent. *Astrophys. J.*, 159:379, 1970. doi: 10.1086/150317.
- V. Rusakov et al. *arXiv e-prints*, art. arXiv:2503.16595, Mar. 2025. doi: 10.48550/arXiv.2503.16595.
- C. G. Sabiu, K. Kadota, J. Asorey, and I. Park. *Journal of Cosmology and Astroparticle Physics*, 2022(01):020, 2022.
- N. Sabti et al. *Machine Learning: Science and Technology*, 6(1):015039, Mar. 2025. doi: 10.1088/2632-2153/adb19c.
- S. Samui, K. Subramanian, and R. Srianand. In *29th International Cosmic Ray Conference (ICRC29), Volume 9*, volume 9 of *International Cosmic Ray Conference*, page 215, Jan. 2005.
- S. Samui, K. Subramanian, and R. Srianand. *MNRAS*, 476(2):1680–1695, May 2018. doi: 10.1093/mnras/sty287.
- M. G. Santos et al. *ApJ*, 689:1, 2008. doi: 10.1086/592487.
- M. G. Santos et al. *A&A*, 527:A93, Mar. 2011. doi: 10.1051/0004-6361/201015695.
- D. Sarkar and E. D. Kovetz. *Phy. Rev. D*, 107(2):023524, Jan. 2023. doi: 10.1103/PhysRevD.107.023524.

- D. Sarkar, J. Flitter, and E. D. Kovetz. *Physical Review D*, 105(10):103529, 2022.
- N. S. Sartorio et al. *MNRAS*, 521(3):4039–4055, May 2023. doi: 10.1093/mnras/stad697.
- K. Sato. *Monthly Notices of the Royal Astronomical Society*, 195(3):467–479, 07 1981. ISSN 0035-8711. doi: 10.1093/mnras/195.3.467. URL <https://doi.org/10.1093/mnras/195.3.467>.
- S. Satyavolu, G. Kulkarni, L. C. Keating, and M. G. Haehnelt. *MNRAS*, 533(1):676–686, Sept. 2024. doi: 10.1093/mnras/stae1717.
- A. Saxena, S. Majumdar, M. Kamran, and M. Viel. *Monthly Notices of the Royal Astronomical Society*, 497(3):2941–2953, 2020.
- S. Sazonov and R. Sunyaev. *MNRAS*, 454(4):3464–3471, Dec. 2015. doi: 10.1093/mnras/stv2255.
- T. Schaeffer, S. K. Giri, and A. Schneider. *MNRAS*, 526(2):2942–2959, 10 2023. doi: 10.1093/mnras/stad2937.
- D. Schaerer. *A&A*, 382:28–42, Jan. 2002. doi: 10.1051/0004-6361:20011619.
- A. T. P. Schauer, B. Liu, and V. Bromm. *ApJL*, 877(1):L5, May 2019. doi: 10.3847/2041-8213/ab1e51.
- A. T. P. Schauer, S. C. O. Glover, R. S. Klessen, and P. Clark. *MNRAS*, 507(2):1775–1787, Oct. 2021. doi: 10.1093/mnras/stab1953.
- P. Schellart et al. *A&A*, 560:A98, Dec. 2013. doi: 10.1051/0004-6361/201322683.
- D. R. G. Schleicher, R. Banerjee, and R. S. Klessen. *Phys. Rev. D*, 78(8):083005, Oct. 2008. doi: 10.1103/PhysRevD.78.083005.
- D. R. G. Schleicher, R. Banerjee, and R. S. Klessen. *Astrophys. J. Letters*, 692(1):236–245, Feb. 2009. doi: 10.1088/0004-637X/692/1/236.
- R. Schlickeiser. *Cosmic Ray Astrophysics*. Springer Berlin, Heidelberg, 2002.
- A. Schneider, S. K. Giri, and J. Mirocha. *Physical Review D*, 103(8):083025, 2021.
- A. Schneider, T. Schaeffer, and S. K. Giri. *Physical Review D*, 108(4):043030, 2023.
- F. G. Schröder. *Progress in Particle and Nuclear Physics*, 93:1–68, 2017. ISSN 0146-6410. doi: <https://doi.org/10.1016/j.pnnp.2016.12.002>. URL <https://www.sciencedirect.com/science/article/pii/S0146641016300758>.
- T. P. Schwandt et al. *arXiv e-prints*, art. arXiv:2505.02716, May 2025. doi: 10.48550/arXiv.2505.02716.
- S. Seager, D. D. Sasselov, and D. Scott. *ApJ*, 523:L1, 1999. doi: 10.1086/312250.
- B. Semelin et al. *Astron. Astrophys.*, 672:A162, 2023. doi: 10.1051/0004-6361/202244722.
- S. K. Sethi and K. Subramanian. *MNRAS*, 356(2):778–788, Jan. 2005. doi: 10.1111/j.1365-2966.2004.08520.x.

- Y. Shao et al. *Nature Astronomy*, 7(9):1116–1126, 2023.
- P. R. Shapiro, I. T. Iliev, and A. C. Raga. *MNRAS*, 348(3):753–782, Mar. 2004. doi: 10.1111/j.1365-2966.2004.07364.x.
- P. R. Shapiro et al. *ApJ*, 646(2):681–690, Aug. 2006. doi: 10.1086/504972.
- P. R. Shapiro et al. *Phy. Rev. Lett.*, 110(15):151301, Apr. 2013. doi: 10.1103/PhysRevLett.110.151301.
- P. Sharda and S. H. Menon. *MNRAS*, 540(2):1745–1764, June 2025. doi: 10.1093/mnras/staf803.
- P. Sharda et al. *MNRAS*, 541(1):L1–L7, July 2025. doi: 10.1093/mnrasl/slaf043.
- R. Sharma et al. *arXiv preprint arXiv:2504.00303*, 2025.
- A. K. Shaw, S. Bharadwaj, and R. Mondal. *MNRAS*, 487(4):4951–4964, 06 2019. ISSN 0035-8711. doi: 10.1093/mnras/stz1561. URL <https://doi.org/10.1093/mnras/stz1561>.
- H. Shimabukuro, K. Ichiki, S. Inoue, and S. Yokoyama. *Physical Review D*, 90(8):083003, 2014.
- H. Shimabukuro, K. Ichiki, and K. Kadota. *Physical Review D*, 102(2):023522, 2020a.
- H. Shimabukuro, K. Ichiki, and K. Kadota. *Physical Review D*, 101(4):043516, 2020b.
- H. Shukla, G. Mellema, I. T. Iliev, and P. R. Shapiro. *MNRAS*, 458(1):135–150, May 2016. doi: 10.1093/mnras/stw249.
- S. Sikder, R. Barkana, and A. Fialkov. *Astrophysical Journal Letters*, 970(2):L25, Aug. 2024a. doi: 10.3847/2041-8213/ad5c5f.
- S. Sikder, R. Barkana, A. Fialkov, and I. Reis. *MNRAS*, 527(4):10975–10985, Feb. 2024b. doi: 10.1093/mnras/stad3847.
- S. Sikder et al. *arXiv e-prints*, art. arXiv:2509.11175, Sept. 2025. doi: 10.48550/arXiv.2509.11175.
- J. Singal et al. *Publications of the Astronomical Society of the Pacific*, 130(985):036001, Mar. 2018. doi: 10.1088/1538-3873/aaa6b0.
- J. Singal et al. *Publ. Astron. Soc. Pac.*, 135:036001, 2023. doi: 10.1088/1538-3873/acbdbf.
- S. Singh et al. *Nature Astronomy*, 6:607–617, Feb. 2022. doi: 10.1038/s41550-022-01610-5.
- M. Sitwell, A. Mesinger, Y.-Z. Ma, and K. Sigurdson. *Monthly Notices of the Royal Astronomical Society*, 438(3):2664–2671, 2014.
- SKA foregrounds chapter. *arXiv preprint arXiv:NNNN.MMMMM*, 2025.
- T. R. Slatyer. *Phys. Rev. D*, 93(2):023527, 2016a. doi: 10.1103/PhysRevD.93.023527.
- T. R. Slatyer. *Phys. Rev. D*, 93(2):023521, 2016b. doi: 10.1103/PhysRevD.93.023521.
- T. R. Slatyer. *Nuc. Phys. B*, 1003:116468, 2024. doi: <https://doi.org/10.1016/j.nuclphysb.2024.116468>.

- T. R. Slatyer, N. Padmanabhan, and D. P. Finkbeiner. *Phys. Rev. D*, 80:043526, 2009. doi: 10.1103/PhysRevD.80.043526.
- A. Stacy and V. Bromm. *MNRAS*, 382(1):229–238, Nov. 2007. doi: 10.1111/j.1365-2966.2007.12247.x.
- A. Stacy, V. Bromm, and A. Loeb. *ApJL*, 730(1):L1, Mar. 2011. doi: 10.1088/2041-8205/730/1/L1.
- A. Starobinsky. *Physics Letters B*, 91(1):99–102, 1980. ISSN 0370-2693. doi: [https://doi.org/10.1016/0370-2693\(80\)90670-X](https://doi.org/10.1016/0370-2693(80)90670-X). URL <https://www.sciencedirect.com/science/article/pii/037026938090670X>.
- R. Subrahmanyan and R. Cowsik. *The Astrophysical Journal*, 776(1):42, Oct 2013. doi: 10.1088/0004-637X/776/1/42.
- R. Subrahmanyan et al. *MNRAS*, 315(4):808–822, July 2000. doi: 10.1046/j.1365-8711.2000.03444.x.
- K. Subramanian. *Reports on Progress in Physics*, 79(7):076901, July 2016. doi: 10.1088/0034-4885/79/7/076901.
- T.-Y. Sun et al. *Communications Physics*, 8(1):1–13, 2025.
- Y. Sun et al. *Phy. Rev. D*, 111(4):043015, Feb. 2025a. doi: 10.1103/PhysRevD.111.043015.
- Y. Sun, J. W. Foster, and J. B. Muñoz. *arXiv e-prints*, art. arXiv:2509.22772, Sept. 2025b. doi: 10.48550/arXiv.2509.22772.
- A. Takahashi et al. *ApJ*, 960(2):112, Jan. 2024. doi: 10.3847/1538-4357/ad045e.
- Y. Takeuchi and S. Chongchitnan. *Monthly Notices of the Royal Astronomical Society*, 439(1): 1125–1135, 02 2014. ISSN 0035-8711. doi: 10.1093/mnras/stu059. URL <https://doi.org/10.1093/mnras/stu059>.
- H. Tashiro and N. Sugiyama. *MNRAS*, 372(3):1060–1068, Nov. 2006. doi: 10.1111/j.1365-2966.2006.10901.x.
- H. Tashiro, K. Kadota, and J. Silk. *Phy. Rev. D*, 90(8):083522, Oct. 2014. doi: 10.1103/PhysRevD.90.083522.
- E. Thélie, F. Del Balso, J. B. Muñoz, and A. Liu. *Phy. Rev. D*, 111(12):123501, June 2025. doi: 10.1103/jfkk-7q7l.
- D. Tseliakhovich and C. Hirata. *Phy. Rev. D*, 82(8):083520, Oct 2010. doi: 10.1103/PhysRevD.82.083520.
- D. Tseliakhovich, R. Barkana, and C. M. Hirata. *MNRAS*, 418(2):906–915, Dec. 2011. doi: 10.1111/j.1365-2966.2011.19541.x.
- M. Tueros, M. V. del Valle, and G. E. Romero. *A&A*, 570:L3, Oct. 2014. doi: 10.1051/0004-6361/201424666.

- A. Venkatesan, M. L. Giroux, and J. M. Shull. *ApJ*, 563(1):1–8, Dec. 2001. doi: 10.1086/323691.
- E. M. Ventura et al. *MNRAS*, 520(3):3609–3625, Apr. 2023. doi: 10.1093/mnras/stad237.
- E. M. Ventura, Y. Qin, S. Balu, and J. S. B. Wyithe. *MNRAS*, 540(1):483–497, June 2025a. doi: 10.1093/mnras/staf699.
- E. M. Ventura, Y. Qin, S. Balu, and J. S. B. Wyithe. *MNRAS*, 540(1):483–497, June 2025b. doi: 10.1093/mnras/staf699.
- T. Venumadhav, L. Dai, A. Kaurov, and M. Zaldarriaga. *Phy. Rev. D*, 98(10):103513, Nov 2018. doi: 10.1103/PhysRevD.98.103513.
- J. Verwohlt et al. *Phys. Rev. D*, 110(10):103533, 2024. doi: 10.1103/PhysRevD.110.103533.
- E. Visbal et al. *Nature*, 487(7405):70–73, July 2012. doi: 10.1038/nature11177.
- M. Volonteri. *A&A Rev.*, 18(3):279–315, July 2010. doi: 10.1007/s00159-010-0029-x.
- I. Wasserman. *Astrophys. J.*, 224:337–343, Sept. 1978. doi: 10.1086/156381.
- J. Wasserman et al. *arXiv e-prints*, art. arXiv:2507.21764, July 2025. doi: 10.48550/arXiv.2507.21764.
- C. A. Watkinson et al. *MNRAS*, 482(2):2653–2669, Jan. 2019. doi: 10.1093/mnras/sty2740.
- D. Whalen, T. Abel, and M. L. Norman. *ApJ*, 610(1):14–22, July 2004. doi: 10.1086/421548.
- D. Whalen, B. van Veelen, B. W. O’Shea, and M. L. Norman. *ApJ*, 682(1):49–67, July 2008. doi: 10.1086/589643.
- J. H. Wise et al. *Nature*, 566(7742):85–88, Jan. 2019. doi: 10.1038/s41586-019-0873-4.
- S. A. Wouthuysen. *Astron. J.*, 57:31–32, 1 1952. doi: 10.1086/106661.
- K. Wu, Q. Han, and J. Y. H. Chan. *MNRAS*, 531(3):3088–3102, July 2024. doi: 10.1093/mnras/stae1311.
- Y. Xu, J. Hamann, and X. Chen. *Phys. Rev. D*, 94(12):123518, 2016. doi: 10.1103/PhysRevD.94.123518.
- Y. Xu, B. Yue, and X. Chen. *ApJ*, 869(1):42, Dec. 2018. doi: 10.3847/1538-4357/aae97b.
- Y. Xu, B. Yue, and X. Chen. *ApJ*, 923(1):98, Dec. 2021. doi: 10.3847/1538-4357/ac30da.
- X. Yang, H. J. Mo, and F. C. van den Bosch. *MNRAS*, 339(4):1057–1080, Mar. 2003. doi: 10.1046/j.1365-8711.2003.06254.x.
- L. Yin, 2023. URL <https://arxiv.org/abs/2305.20038>.
- S. Yoshiura, K. Takahashi, and T. Takahashi. *Phys. Rev. D*, 98(6):063529, 2018. doi: 10.1103/PhysRevD.98.063529.
- S. Yoshiura, K. Takahashi, and T. Takahashi. *Phys. Rev. D*, 101(8):083520, 2020. doi: 10.1103/PhysRevD.101.083520.

- B. Yue, A. Ferrara, and Y. Xu. *MNRAS*, 463(2):1968–1979, Dec. 2016. doi: 10.1093/mnras/stw2145.
- B. Yue, A. Ferrara, F. Pacucci, and K. Omukai. *ApJ*, 838(2):111, Apr. 2017. doi: 10.3847/1538-4357/aa6627.
- B. Yue et al. *ApJ*, 868(2):115, Dec. 2018. doi: 10.3847/1538-4357/aae77f.
- E. Zackrisson et al. *Monthly Notices of the Royal Astronomical Society*, 493(1):855–870, 2020.
- P. Zarrouk et al. *MNRAS*, 477(2):1639–1663, June 2018. doi: 10.1093/mnras/sty506.
- K. Zawada et al. *MNRAS*, 439(2):1615–1627, Apr. 2014. doi: 10.1093/mnras/stu035.
- J.-F. Zhang, B. Wang, and X. Zhang. *Science China Physics, Mechanics, and Astronomy*, 63(8): 280411, Aug. 2020. doi: 10.1007/s11433-019-1516-y.
- X. Zhang et al. *ApJ*, 964(1):62, Mar. 2024. doi: 10.3847/1538-4357/ad235b.